nature neuroscience

Stimulation of the insulin/mTOR pathway delays cone death in a mouse model of retinitis pigmentosa

Claudio Punzo[1], Karl Kornacker[2] & Constance L Cepko[1,3]

Retinitis pigmentosa is an incurable retinal disease that leads to blindness. One puzzling aspect concerns the progression of the disease. Although most mutations that cause retinitis pigmentosa are in rod photoreceptor–specific genes, cone photoreceptors also die as a result of such mutations. To understand the mechanism of non-autonomous cone death, we analyzed four mouse models harboring mutations in rod-specific genes. We found changes in the insulin/mammalian target of rapamycin pathway that coincided with the activation of autophagy during the period of cone death. We increased or decreased the insulin level and measured the survival of cones in one of the models. Mice that were treated systemically with insulin had prolonged cone survival, whereas depletion of endogenous insulin had the opposite effect. These data suggest that the non-autonomous cone death in retinitis pigmentosa could, at least in part, be a result of the starvation of cones.

Retinitis pigmentosa is a type of inherited retinal degeneration. It is currently untreatable and usually leads to blindness. With over 40 reintitis pigmentosa genes identified, it is the most common type of retinal degeneration caused by a single disease allele (RetNet, http://www.sph.uth.tmc.edu/Retnet/). The phenotype is characterized by an initial loss of night vision as a result of the malfunction and death of rod photoreceptors. This phase is followed by a progressive loss of cones. Because cones are responsible for color and high-acuity vision, it is their loss that leads to a reduction in the quality of life. In many cases, the disease-causing allele is expressed exclusively in rods; nonetheless, cones die as well. Indeed, to date there is no known form of retinal degeneration in humans or mice where rods die and cones survive. In contrast, mutations in cone-specific genes result only in cone death. Several theories have been proposed to explain this finding. For example, cone death could be a result of the release of a toxin produced by dying rods or the loss of a trophic factor that is produced by healthy rods[1–6]. Alternatively, cone death could be caused by microglia that are mobilized initially during rod death[7] or by oxidative stress[8,9]. Oxidative stress might also directly harm cones. The constant flow of oxygen through the retinal pigmented epithelium (RPE) to photoreceptors and the loss of rods, which are 95% of the photoreceptors in human and mouse, may result in an overload of oxygen to the remaining cones[10]. Evidence for all of these mechanisms exists in mice, yet none are able to fully explain why cones may survive for many years in the absence of rods in humans. Nonetheless, rodents are a very good model for this type of retinal degeneration. Although the rodent retina lacks a macula, which is the cone-rich and rod-free area that is present in humans, the macula is not involved in the initial phase of the disease. In humans, retinitis pigmentosa starts outside of the macula, where the distribution of rods and cones is similar to that in mice.

To determine the common underlying mechanism for cone death in retinitis pigmentosa, we compared four mouse models harboring mutations in rod-specific genes (*Pde6b*$^{-/-}$ (ref. 11), *Pde6g*$^{-/-}$ (ref. 12), *Rho*$^{-/-}$ (ref. 13) and P23H[14], which carries a *Rho* transgene that has an amino acid subsitution of histidine for proline at amino acid 23, as occurs in some human cases of retinitis pigmentosa, see Methods). Affymetrix arrays were used to identify common changes in gene expression that accompany cone death. Changes in a substantial number of genes involved in cellular metabolism coincided with the onset of cone death. These changes were suggestive of cones suffering from a shortage of nutrients. We then found that cones showed signs of autophagy, a cellular self-digestion process, which is consistent with prolonged starvation. We also found that several aspects of the insulin/mammalian target of rapamycin (mTOR) pathway, an important pathway that regulates cellular metabolism, were affected during the period of cone degeneration. As a result of this finding, we increased and decreased the insulin level and measured the survival of cones in one of the models. Mice treated systemically with insulin had prolonged cone survival, whereas depletion of endogenous insulin had the opposite effect. Therefore, cone starvation is a likely contributor to the slow demise of cones in humans with retinitis pigmentosa. Treatments aimed at improving nutrition of cones are thus a plausible therapeutic avenue.

RESULTS

Photoreceptor death kinetics and microarray analysis

To establish a framework for comparing gene expression in four different models of retinitis pigmentosa, we established the equivalent stages of disease pathology through examination of the kinetics of rod (**Fig. 1** and **Supplementary Figs. 1** and **2** online) and cone (**Fig. 2** and

[1]Harvard Medical School, Department of Genetics and Howard Hughes Medical Institute, 77 Avenue Louis Pasteur, Boston, Massachusetts 02115, USA. [2]The Research Institute at Nationwide Children's Hospital and the Ohio State University, 169 Westwood Road, Columbus, Ohio 43214, USA. [3]Department of Ophthamology, Harvard Medical School, 77 Avenue Louis Pasteur, Boston, Massachusetts 02115, USA. Correspondence should be addressed to C.L.C. (cepko@genetics.med.harvard.edu).

Received 30 September; accepted 30 October; published online 7 December 2008; doi:10.1038/nn.2234

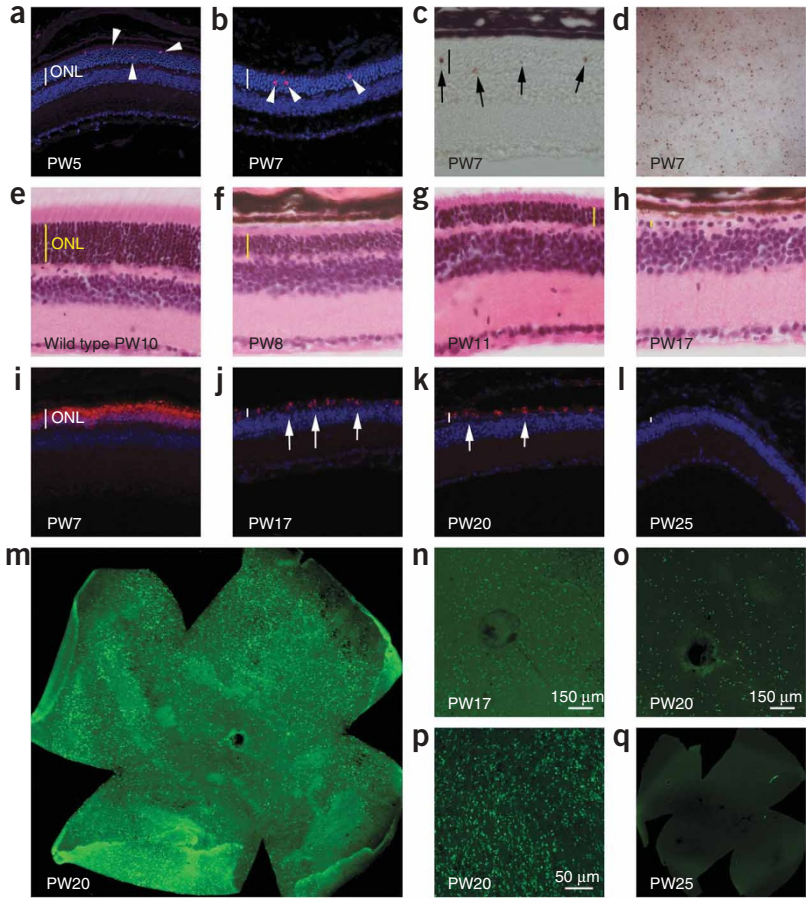

Figure 1 Rod death kinetics in the *Rho*$^{-/-}$ mouse. All panels show *Rho*$^{-/-}$ mice with the exception of **e**. (**a**–**d**) Onset of rod death visualized by staining for cleaved nuclear envelope protein LaminA (**a**), cleaved caspase3 (arrowheads, magenta and red signal, **b**) and TUNEL (arrows, brown signal, **c**,**d**). Blue in **a** and **b** shows nuclear DAPI staining. A retinal flat mount with a view onto the photoreceptor layer is shown in **d**. (**e**–**h**) Progression of rod death determined by the reduction of the ONL was visualized by hematoxylin and eosin staining. (**i**–**q**) End phase of rod death was assessed by section analysis (**i**–**l**) or by retinal flat mounts (**m**–**q**). In the *Rho*$^{-/-}$ mouse, the onset of rod death was around PW5 (**a**) and progressed up to PW25 (**l**). By PW17, the ONL was reduced to one row of cells (**h**,**j**) and the remaining rods died in the following 8 weeks (**j**–**q**), as seen by immunofluorescence with an antibody to Gnat1 on sections of progressively older animals (**j**–**l**). Retinal flat mounts showing rods visualized by immunofluorescence with an antibody Gnat1 are shown in **m**–**q**. The entire retina is shown in **m**, higher magnifications around the optic nerve head are shown in **n** and **o**, and the peripheral region is shown in **p**. No signal was seen at PW25 on flat mounts (**q**) or sections (**l**). Age (in PW) is indicated in the panels. Vertical bar in **a**–**c** and **e**–**l** indicates thickness of the ONL.

Supplementary Fig. 3 online) death. Rod death kinetics was established by determining the onset, progression and end phase of rod death (**Fig. 1**). The time from the onset of rod death to the time when the outer nuclear layer (ONL) was reduced to one row of cells is referred to as the major rod death phase. The time thereafter until rod death was complete will be referred to as the end phase of rod death. To determine the beginning of the major phase of rod death, we examined the cleavage of the nuclear envelope protein LaminA (**Fig. 1a**) and of the apoptotic protease caspase3 (**Fig. 1b**), and used TUNEL staining (**Fig. 1c**,**d**). The continuation of the major rod death phase was monitored by these assays, as well as inspection of histological sections (**Fig. 1e–h**), as rods account for more than 95% of all photoreceptors. Once the ONL reached one row of cells, the major phase of rod death was over. The end phase of rod death was determined using rod-specific markers to perform either *in situ* hybridization (**Supplementary Fig. 1**) or immunohistochemistry (**Fig. 1i–l**) on retinal sections. However, it is difficult to determine whether any rods remain unless every section of a single retina is collected. Thus, retinal flat mounts were also used to allow a comprehensive analysis of the end phase of rod death (**Fig. 1m–q**). Notably, although the end phase of rod death was clearly defined in the two cGMP phosphodiesterase (PDE) mutants and in the *Rho*$^{-/-}$ mutant, rods died so slowly in the P23H mutant that some rods were still present even 50 weeks (latest time point analyzed) after the end of the major phase of rod death (**Supplementary Fig. 2**).

We used two methods to determine the onset and progression of cone death. First, the overall time frame of cone demise was determined by quantitative real-time PCR (qRT-PCR; **Fig. 2a**) for the ventral[15] cone–specific transcript *Opn1sw* (opsin1 short-wave sensitive, blue cone opsin). This allowed for an initial quantitative comparison among different strains, but was not adequate to determine the number of cones, as transcript levels could vary before cell death. Next, we used whole-mount immunohistochemistry for red/green opsin (*Opn1mw*, opsin1 medium-wave sensitive) and peanut agglutinin lectin (PNA) (**Fig. 2b–n**). Both markers were expressed throughout the murine retina, allowing for the visualization of cones (**Fig. 2b–d**). Notably, the onset of cone death always occurred at the equivalent stage of rod death, namely after the major rod death phase, when the thickness of the ONL was reduced to only a single row of cells. We found that cone death occurred from the center to the periphery in all four models, as seen by staining with PNA (**Fig. 2e**). It was preceded by a gradual reduction of the outer segment length (**Fig. 2f–i**) and by opsin localization from the outer segment to the entire cell membrane (**Fig. 2j–l**). In addition, red/green opsin protein, which is normally detected throughout the mouse retina (**Fig. 2b**), was detected mainly dorsally during cone degeneration (**Fig. 2m**,**n**). However, PNA staining showed no appreciable difference across the dorsal/ventral axis (**Fig. 2m**,**n**). Similarly, blue opsin expression, which is normally detected only ventrally[15] (**Fig. 2c**,**d**), was not affected during this early phase of cone degeneration (**Fig. 2o**). Shortening of cone outer segments and loss of cone-specific markers has also been described in human cases of retinitis pigmentosa[16].

In summary, the kinetics and histological changes that accompanied rod and cone death shared several features across the four models. First, cone degeneration always started after the end of the major rod death phase (**Fig. 3a**,**b**). This point was reached at very different ages in three of the four mutants, as the overall kinetics of rod death were quite different. Second, cone death was always central to peripheral and was preceded by a reduction in outer segment length. Third, in all four mutants, red/green opsin protein levels were detectable mainly dorsally during cone degeneration (**Fig. 3c**). These common features suggested

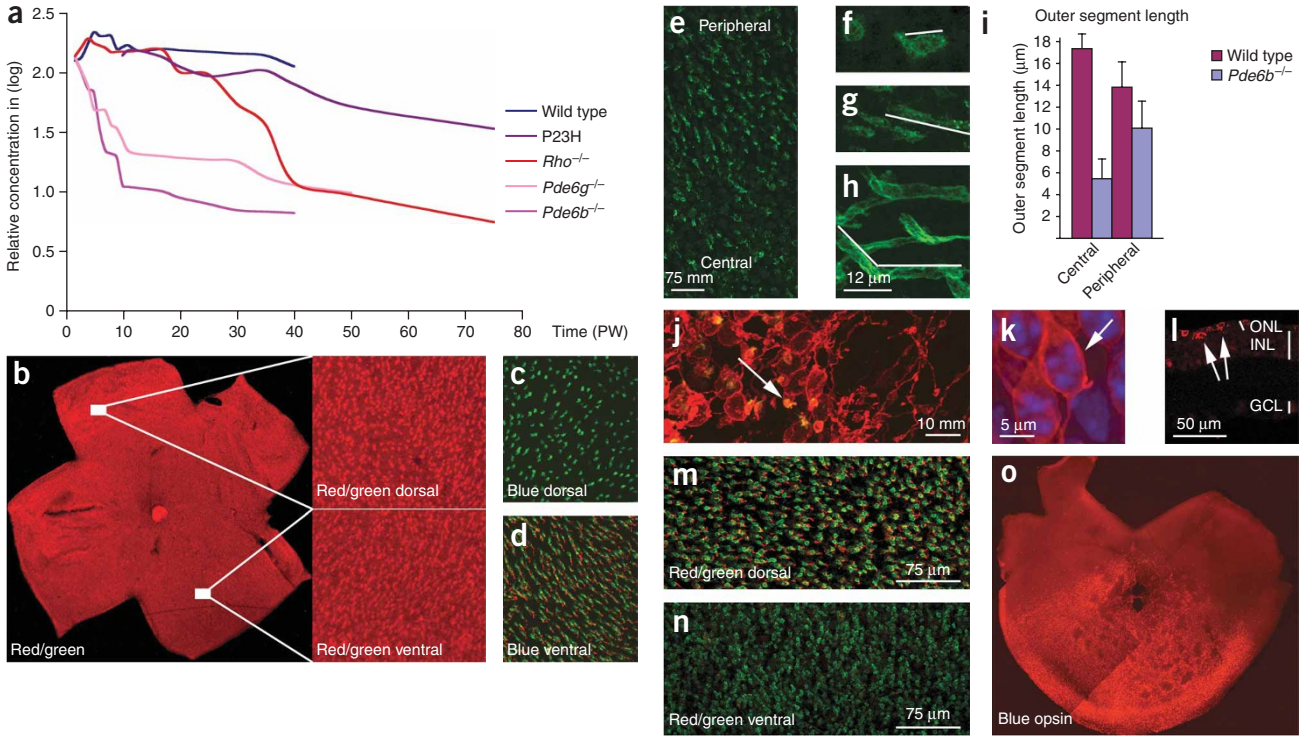

Figure 2 Cone death kinetics. (**a**) qRT-PCR analysis for *Opn1sw* during cone degeneration. (**b**–**o**) All panels show retinal flat mounts except for **i** and **l**. Green signal indicates PNA expression and red signal indicates red/green or blue opsin. The wild-type retina is shown at P35 in **b**–**d**. Red/green opsin (**b**) and PNA (**c**,**d**) expression were detected both dorsally and ventrally, whereas blue opsin (**c**,**d**) was detected only ventrally. The *Pde6b*$^{-/-}$ mouse is analyzed in **e**–**g** and **j**–**o**. A central to peripheral gradient of PNA and shortening of cone outer segments is shown in **e**–**g**. At P20, there were fewer elongated outer segments in the center (**e**) as compared with the periphery. Higher magnifications of a central or peripheral outer segment from **e** are shown in **f** and **g**, and a wild-type outer segment is shown in **h** (white line marks the outer segment). A quantification of outer segment length at 3 weeks is shown in **i** (error bars represent s.d. of 15 measurements each). With the shortening of outer segments during degeneration, red/green opsin was localized throughout the membrane of the cell body, and PNA, which detects an extracellular protein(s), was reduced to a small dot attached to the residual outer segment (**j**) (yellow shows red/green and PNA overlap, arrow). A higher magnification of a cone showing red/green at the membrane is displayed in **k** (arrow). A cross section showing red/green in cell body is shown in **l** (arrows) (P70; **j**–**l**). During degeneration, red/ green opsin was detected mainly dorsally (**m**), whereas PNA (**m**, **n**) or blue opsin (**o**) expression were not altered (**m** and **n**, P21; **o**, P49). GCL, ganglion cell layer; INL, inner nuclear layer.

that there might be a common mechanism(s) of cone death and that clues about this mechanism(s) might be suggested by gene expression changes that were common across the four models at the onset of cone death.

To determine common gene expression changes, we collected RNA samples from all four models halfway through the major phase of rod death, at the onset of cone death and from two time points during the cone death phase (**Fig. 4a**). The RNA was hybridized to an Affymetrix 430 2.0 mouse array. Gene expression changes were compared in the same strain across the four time points. Two criteria had to be fulfilled to select a gene for cross comparison among the four strains. First, the change over time had to be statistically significant (see Methods, $P < 0.01$). Second, a gene had to be upregulated at least twofold at the onset of cone death compared with the other three time points. This second criterion removed rod-specific changes that were still occurring at the onset of cone death and at the same time enriched for changes at the onset of cone death. A total of 240 Affymetrix ID numbers were found that satisfied both criteria in each of the four strains. The 240 ID numbers matched to 230 genes (**Supplementary Table 1** online). Of the 195 genes that could be annotated, 34.9% (68 genes) were genes that are involved in cellular metabolism (**Fig. 4b**,**c**). The signaling pathway with the highest number of hits (12 genes) was the insulin/mTOR signaling pathway (**Fig. 4b**), an important pathway for regulating many aspects of cellular metabolism. Thus, the data suggested that events at the onset of cone death coincided with changes in cellular metabolism that might be regulated by the insulin/mTOR pathway.

mTOR in wild-type and degenerating retinae

On the basis of our findings from the microarray analysis, we examined the insulin/mTOR signaling pathway during the period of cone death. The kinase mTOR is an important regulator of protein synthesis and ribosome biogenesis[17]. When cellular energy levels are high, mTOR allows energy-consuming processes such as translation, and prevents autophagy, whereas mTOR has a reverse effect in nutrient-poor conditions. Therefore, glucose, which increases cellular ATP levels, and amino acid availability, especially that of leucine, positively affects mTOR activity. To begin to investigate the activity level of mTOR during degeneration, we examined levels of phosphorylated mTOR (P-mTOR) by immunofluorescence. Phosphorylation of mTOR increases kinase activity and P-mTOR levels can therefore serve as an indicator of its activity level. Because every eukaryotic cell expresses mTOR, a certain level of P-mTOR is likely to be found in every cell. Notably, high levels of P-mTOR were detected only in dorsal cones of wild-type retinae (**Fig. 5a**–**c**). Notably, this pattern of P-mTOR is reminiscent of the red/green opsin pattern that was seen during cone degeneration (**Fig. 3c**).

We investigated whether the ventral red/green opsin downregulation that occurred during cone degeneration could be mimicked by a

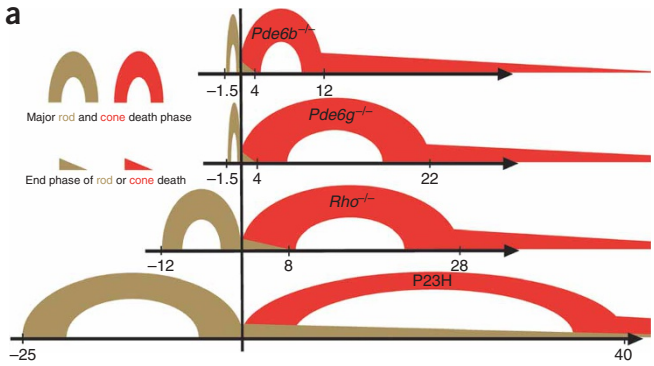

b

Strain	Major rod death phase	End phase of rod death	Major cone death phase	End phase of cone death
Pde6b$^{-/-}$	P11–20	PW3–7	PW3–15	present at PW45
Pde6g$^{-/-}$	P11–20	PW3–7	PW3–15	present at PW45
Rho$^{-/-}$	PW5–17	PW17–25	PW17–45	present at PW80
P23H	PW10–35	present at PW80	PW35 on	present at PW80

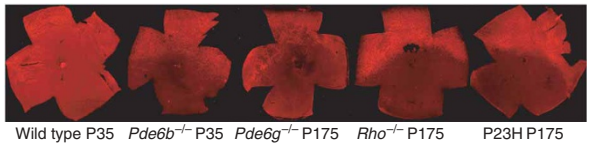

Figure 3 Summary of rod and cone death kinetics. (**a**) Schematic representation of the rod and cone death kinetics found in the four mouse models of retinitis pigmentosa. The onset of cone death is set as time zero. The corresponding time windows on the *x* axis are given in weeks. The major cone death phase was the time period from onset until roughly 85% of cones had died. The end phase of cone death was the time period thereafter. (**b**) Summary of rod and cone death kinetics. Time is indicated in postnatal days or weeks. (**c**) Immunofluorescence on retinal flat mounts showing the ventral reduction of red/green opsin expression found in the four mutants during cone degeneration. Strain and time, in postnatal days, are indicated below each image (for higher magnification of wild type, see **Fig. 2b**).

reduction in mTOR activity. To this end, we treated wild-type mice with rapamycin, an mTOR inhibitor[17]. This treatment resulted in ventral downregulation of red/green opsin without affecting blue opsin or the PNA staining or dorsal phosphorylation of mTOR (**Fig. 5d–g**). Thus, inhibition of mTOR in wild type recapitulated the expression pattern of red/green opsin and blue opsin, as well as the pattern of PNA staining, that was seen in the mutants during degeneration, suggesting that the ventral downregulation of red/green opsin seen during degeneration might be the result of reduced mTOR activity. As expected for mTOR function, the downregulation of red/green opsin did not occur at the RNA level, but instead at the protein level, in untreated mutant mice, as well as in wild-type mice treated with rapamycin (**Supplementary Fig. 4** online). Finally, analysis of mutant retinae showed a decrease of P-mTOR levels in dorsal cones during cone degeneration (**Fig. 5h–m**). To test whether the high level of P-mTOR found in dorsal wild-type cones was glucose-dependent, retinal explants of wild-type mice were cultured in medium for 4 h in the presence or absence of glucose. Dorsal P-mTOR was abolished in the absence of glucose, even when leucine concentrations were increased in the medium (**Supplementary Fig. 5** online). Thus, our data establish a link between mTOR activity, the expression changes of red/green opsin seen during degeneration, and the microarray data, which suggested metabolic changes at the onset of cone death. The changes might be caused by compromised glucose uptake in cones.

Responses of cones to nutritional imbalance

Our mTOR phosphorylation data suggested that a nutritional imbalance was occurring in cones during degeneration, which was possibly caused by reduced glucose levels in cones. To test this idea, we examined the level of the heterodimeric transcription factor hypoxia inducible factor 1 (HIF-1α/β), which improves glycolysis under stress conditions such as low oxygen. HIF-1 and mTOR are tightly linked, as low oxygen results in low energy as a result of reduced oxidative phosphorylation, leading to reduced mTOR activity[17–22]. An upregulation of the regulated subunit HIF-1α would probably reflect low glucose levels in cones and not hypoxic conditions, as oxygen levels are increased as a result of the loss of rods[10]. Immunofluorescence analysis of HIF-1α during cone degeneration revealed an upregulation of the protein in the cones of all four mouse models (**Fig. 6a–f** and **Supplementary Fig. 6** online). Consistent with the upregulation of HIF-1α, glucose transporter 1 (GLUT1, *Slc2a1*), a HIF-1α target gene[23,24] also was found to be upregulated in cones, again in all four mouse models (**Fig. 6g–j** and **Supplementary Fig. 6**). Thus, upregulation of HIF-1α and GLUT1 in cones are consistent with a response to a shortage of glucose. This also provides a link to the decreased P-mTOR levels that we observed during degeneration and to the sensitivity of P-mTOR to glucose.

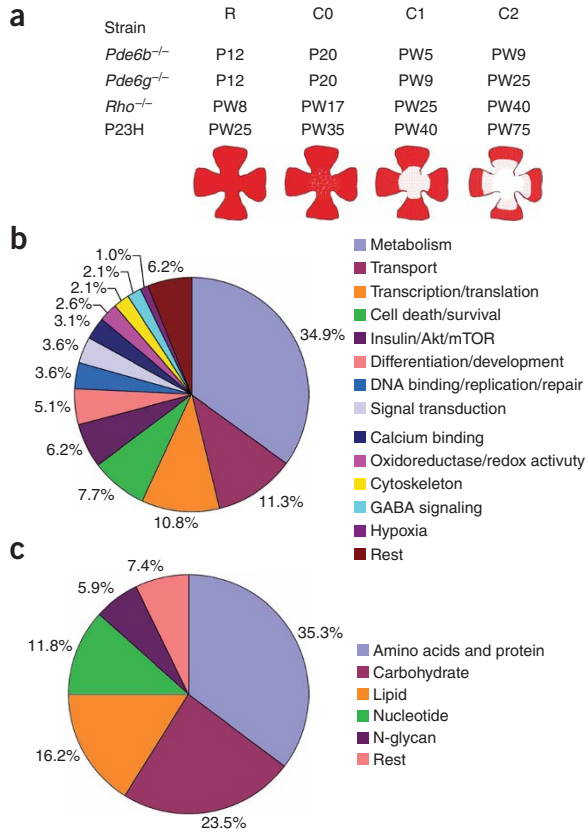

Figure 4 Affymetrix microarray analysis. (**a**) Equivalent time points in the four different mutants at which the microarray analysis was performed (R, approximately halfway through the major phase of rod death; C0, onset of cone death; C1 and C2, first and second time point during cone death, respectively). Time is indicated in postnatal days weeks. Cartoons depicting the progression of cone death are shown below the corresponding time points. (**b**) Distribution in percentages of the 195 genes that were annotated. (**c**) Distribution in percentages of the 68 genes (34.9%) that are part of the metabolism category shown in **b**.

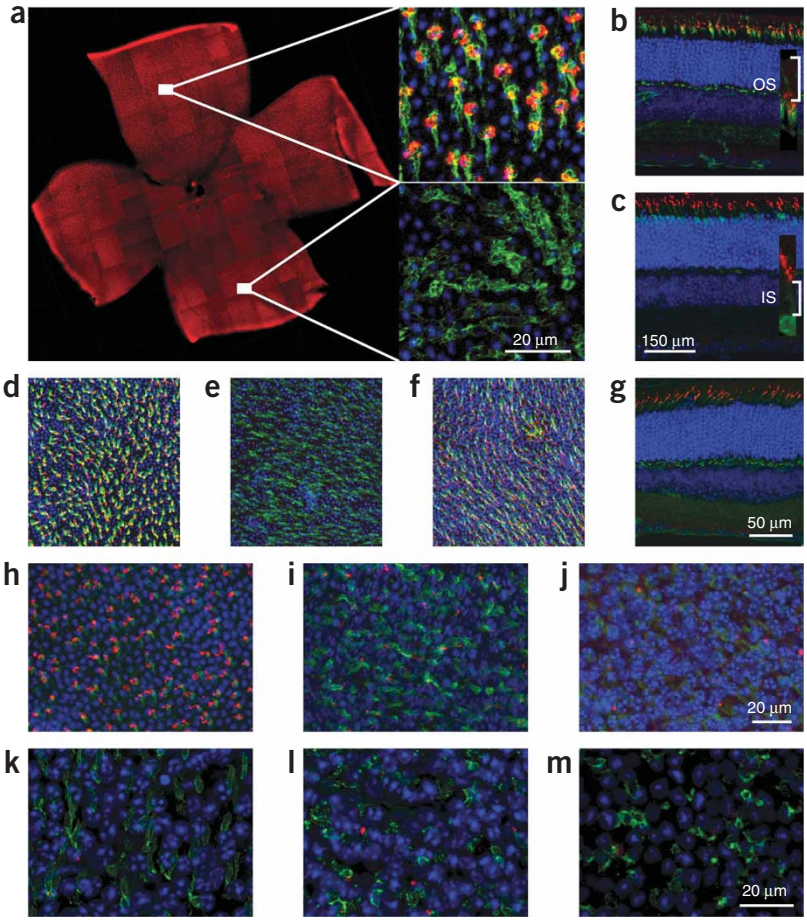

Figure 5 P-mTOR in wild-type and degenerating retinae. (**a**–**c**) P-mTOR levels in wild-type retinae. Dorsal (top) enrichment of P-mTOR (**a**). Higher magnifications of the dorsal and ventral regions are shown to the right, with P-mTOR in red and cone segments in green, as detected by PNA. Dorsal retinal sections stained for P-mTOR (red) and PNA (**b**) or antibody to β-galactosidase (green, **c**). Higher magnification (insets) images suggest that the P-mTOR signal is located in the lower part of the outer segment (OS). IS, inner segment. (**d**–**g**) Rapamycin treatment of wild-type mice led to downregulation of red/green opsin ventrally (**e**) but not dorsally (red, **d**). Ventral blue opsin (red, **f**) remained unaffected, as did PNA (**d**–**g**) (green) and P-mTOR itself (red, **g**). (**h**–**m**) Reduced levels of dorsal P-mTOR during photoreceptor degeneration (red). The wild-type control is shown in **h** and the *Pde6b* mutant is shown in **i** and **j**. Reduction started during rod death at P15 (**i**) as the outer segments (green, PNA) detached from the retinal pigmented epithelium. By P30, only a few cones (green signal: α-*β-galactosidase*) showed high levels of P-mTOR (red) (**j**). (**k**–**m**) Similar reduction was seen in dorsal cones of the other three mutants (cones marked in green by PNA; *Pde6g*$^{-/-}$ is shown at P35 in **k**; *Rho*$^{-/-}$ is shown at PW20 in **l**; P23H is shown at PW70 in **m**). All panels show immunofluorescence on retinal flat mounts (photoreceptor side up) with the exception of **b**, **c** and **g**, which show retinal sections. Blue indicates DAPI.

To ascertain whether cones are nutritionally deprived, we assessed autophagy in cones. Two types of autophagy are inducible by various degrees of nutrient deprivation: macroautophagy and chaperone-mediated autophagy (CMA)[25–28]. Macroautophagy is nonselective, targets proteins or entire organelles, and is marked by *de novo* formation of membranes that form intermediate vesicles (autophagosomes) that fuse with the lysosomes. The machinery required for macroautophagy has been shown to be present in photoreceptors[29]. In contrast, CMA is selective and targets individual proteins for transport to the lysosomes. We assessed the presence of macroautophagy by infection with a viral vector encoding a fusion protein of green fluorescent protein (GFP) and light chain 3 (LC3), an autophagosomal membrane marker[30–32]. No difference was observed in GFP distribution in cones of wild-type and mutant mice, suggesting that formation of autophagosomes was

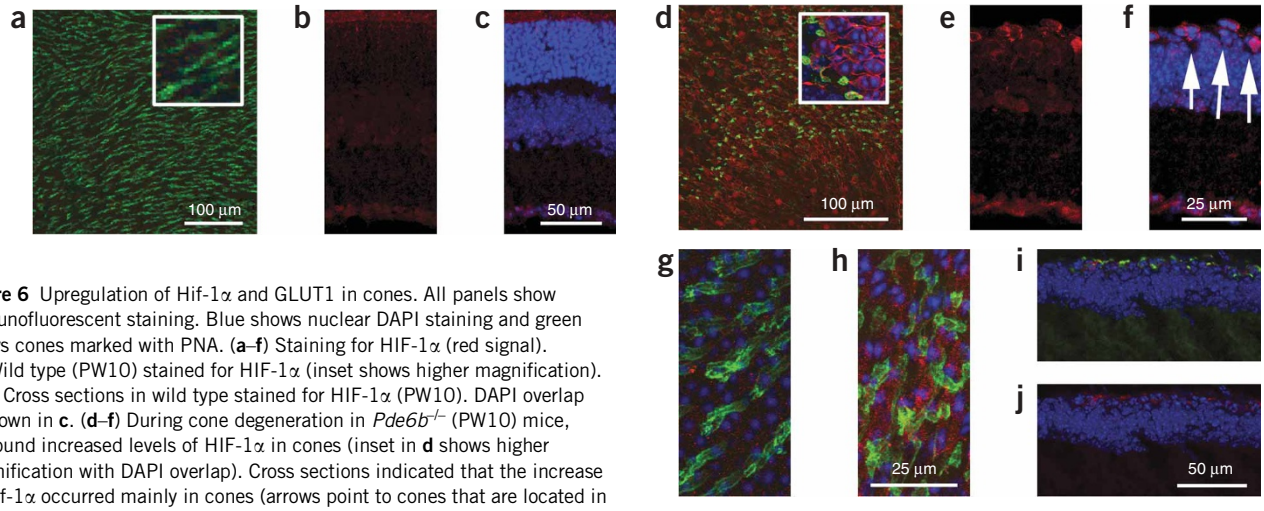

Figure 6 Upregulation of Hif-1α and GLUT1 in cones. All panels show immunofluorescent staining. Blue shows nuclear DAPI staining and green shows cones marked with PNA. (**a**–**f**) Staining for HIF-1α (red signal). (**a**) Wild type (PW10) stained for HIF-1α (inset shows higher magnification). (**b**,**c**) Cross sections in wild type stained for HIF-1α (PW10). DAPI overlap is shown in **c**. (**d**–**f**) During cone degeneration in *Pde6b*$^{-/-}$ (PW10) mice, we found increased levels of HIF-1α in cones (inset in **d** shows higher magnification with DAPI overlap). Cross sections indicated that the increase of Hif-1α occurred mainly in cones (arrows point to cones that are located in the top layer of the inner nuclear layer at this stage; **e**). DAPI overlap is shown in **f**. (**g**) GLUT1 expression in wild type (PW10) (red). Most of the signal in between the cones reflects expression in rods. (**h**–**j**) Increased expression of GLUT1 in cones during degeneration seen in flat mounts (**h**) and sections (**i**,**j**). PNA overlap of **j** is shown in **i**. Retinal flat mounts are shown in **a**, **d**, **g** and **h**. Retinal sections are shown in **b**, **c**, **e**, **f**, **i** and **j**.

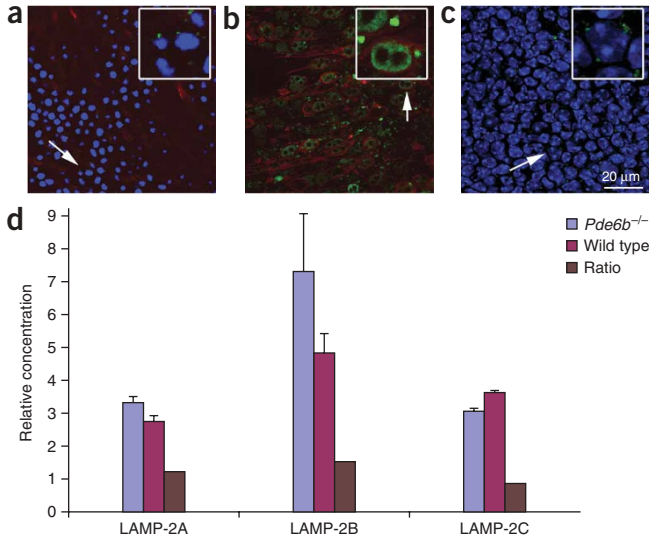

Figure 7 Increased levels of LAMP-2 at the lysosomal membrane. (**a**–**c**) Immunofluorescence on retinal flat mounts (LAMP-2 is shown in green, red/green opsin in red and DAPI in blue). Insets show enlarged cells (arrow). A wild-type retinae at PW5 showing a lysosome (small green dots) with normal LAMP-2 distribution is imaged in **a**. Weak red/green opsin signal was detected at the level of the photoreceptor nuclei, as it was mainly found in the outer segments in the wild type. Enlarged lysosomes (dots) resulting from an accumulation of LAMP-2 at the lysosomal membrane were seen specifically in cones from *Pde6b*$^{-/-}$ mice PW5 (**b**). Confocal section of same field as in **b** taken at the level of the inner nuclear layer showed LAMP-2 levels similar to those in wild type (**c**). (**d**) qRT-PCR for the three different LAMP-2 splice forms showing the relative concentration and the ratios between the *Pde6b*$^{-/-}$ mutant and wild type. Error bars represent s.d. of three measurements.

absent during cone death (**Supplementary Fig. 7** online). In addition, high levels of phosphorylated ribosomal protein S6 were found in all or most cones (**Supplementary Fig. 7**), reflecting an increased activity of ribosomal S6 kinase 1 (S6K1), an inhibitor of macroautophagy[27]. Consistent with these findings is the fact that macroautophagy reflects an acute short-term response to nutrient deprivation or cellular stress conditions[25,26]. Prolonged nonselective degradation of newly synthesized proteins to overcome the stress condition would not be favorable to cells and would probably result in the relatively rapid death of most cones, rather than the slow death that is seen in retinitis pigmentosa.

CMA is normally activated during extended periods of starvation and results in increased levels of lysosomal-associated membrane protein type 2A (LAMP-2A) at the lysosomal membrane[25,26,33]. Both starvation and oxidative stress can induce CMA[25]. Starvation increases LAMP-2A expression by preventing its degradation while oxidative stress results in *de novo* synthesis of LAMP-2A[34]. A LAMP-2 antibody that recognizes the proteins resulting from all three splice isoforms[35] (A, B and C) indicated that there were high levels of LAMP-2 at the lysosomal membrane in all four mutants during cone degeneration (**Fig. 7a–c**; only data for *Pde6b*$^{-/-}$ is shown). The high levels were specific to cones and were not seen in cells of the inner nuclear layer (**Fig. 7b,c**), which might suggest that cones are the only starving cells in the retinitis pigmentosa retina. qRT-PCR for the three splice isoforms showed only a minor increase in mRNA levels of LAMP-2A (1.2-fold) and a decrease in LAMP-2C expression (**Fig. 7d**), suggesting that the increase seen in protein at the membrane is mainly the result of nutritional deprivation, and only to a lesser extent to oxidative stress[8,9,34]. Taken together, the data suggest that nutritional imbalance in cones leads to the activation of CMA, a process that is consistent with prolonged starvation.

Our findings in relation to mTOR, HIF-1α, GLUT1 and the induction of CMA suggested that a shortage of glucose in cones was occurring, resulting in starvation, and suggested that the insulin/mTOR pathway is important during cone death. To determine whether the insulin/mTOR pathway can influence cone survival, we stimulated the pathway by systemic treatment of *Pde6b*$^{-/-}$ mice with insulin. The *Pde6b* mutant was chosen over the other three mutants because of its faster cone death kinetics. Mice were treated with daily intraperitoneal injections of insulin over a 4-week period, starting at the onset of cone

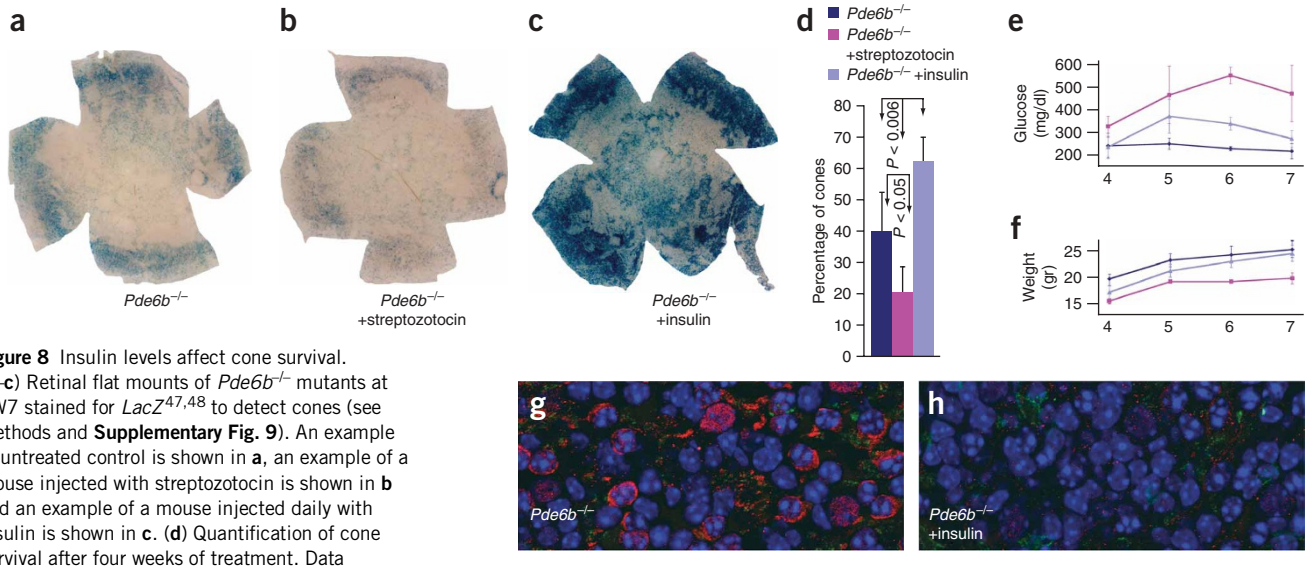

Figure 8 Insulin levels affect cone survival. (**a**–**c**) Retinal flat mounts of *Pde6b*$^{-/-}$ mutants at PW7 stained for *LacZ*[47,48] to detect cones (see Methods and **Supplementary Fig. 9**). An example of untreated control is shown in **a**, an example of a mouse injected with streptozotocin is shown in **b** and an example of a mouse injected daily with insulin is shown in **c**. (**d**) Quantification of cone survival after four weeks of treatment. Data represents an average of at least eight retinae. The *y* axis represents the percentage of the cone surface area versus the surface area of entire retina (see **Supplementary Figs. 8** and **10**). (**e**,**f**) Measurements of blood glucose levels (**e**) and body weight (**f**) performed weekly over the time span of the experiment. (**g**,**h**) Immunofluorescent staining on retinal flat mounts for HIF-1α (red) and PNA (green) in untreated control *Pde6b*$^{-/-}$ (**g**) and *Pde6b*$^{-/-}$ mice treated for 4 weeks with insulin (**h**). DAPI is shown in blue. Error bars in **d**–**f** represent s.d.

death. To reduce insulin, we injected mice with streptozotocin, a drug that kills the insulin-producing beta cells of the pancreas. Systemic administration of insulin results in a desensitized insulin receptor as a result of a feedback loop in the pathway, which causes an increase in blood glucose levels. Injection of streptozotocin, which also results in increased blood glucose levels, served as a control for the effect of elevated blood glucose, and also provided animals with reduced levels of insulin. *Pde6b*$^{-/-}$ mice that were injected with insulin showed improved cone survival compared with non-injected control mice. *Pde6b*$^{-/-}$ mice that were injected with streptozotocin showed a decrease in cone survival (**Fig. 8a–d**). Improved cone survival was therefore a result of insulin and not of the increased blood glucose levels (**Fig. 8e**). Also, insulin treatment did not alter the overall gain in body weight (**Fig. 8f**). In addition, cones in mutant mice that were treated with insulin did not show the upregulation of HIF-1α that is normally seen in cones during degeneration, consistent with the notion that cones were responding to insulin directly (**Fig. 8g**,**h**).

DISCUSSION

Here, we found that cones show signs of nutritional imbalance during the period of cone degeneration in mice with retinitis pigmentosa. Our microarray analysis suggested that there are changes in cellular metabolism that involve the insulin/mTOR pathway at the onset of cone death. We found that inhibition of mTOR in wild-type mice resulted in the same pattern of loss of red/green opsin as is seen during degeneration. Consistent with changes in P-mTOR and its sensitivity to glucose, we observed an upregulation of HIF-1α and GLUT1, suggesting that glucose uptake and/or the intracellular levels of glucose may be compromised in cones of mice with retinitis pigmentosa. In addition, systemic administration of insulin prolonged cone survival, whereas depletion of endogenous insulin had the reverse effect. Systemic treatment with insulin prevented the upregulation of HIF-1α in cones that is normally seen during cone degeneration, suggesting that insulin was directly acting on cones.

We also treated a group of *Pde6b*$^{-/-}$ mutant mice with insulin for 7 weeks, rather than for only 4 weeks. This prolonged treatment with insulin did not show any substantial improvement relative to untreated mutant mice (**Supplementary Fig. 8** online). The difference in cone survival between the two lengths of treatment may reflect the feedback loop of the pathway, in which S6K1 acts directly on the insulin-receptor substrate. Alternatively, or in addition, signaling through the insulin receptor might slow down autophagy, but would not address a fundamental problem, such as insufficient glucose. Eventually, the cones died, perhaps in an accelerated fashion once their metabolic demands exceeded the supply. An acceleration of cone death might be predicted, if in fact insulin suppressed autophagy, and thereby created more of an energy imbalance. Although the cross talk in cones between the insulin receptor, mTOR, HIF-1α, S6K1 and insulin-receptor substrate remains to be investigated, the results strengthen the notion that nutrient availability in cones may be altered during the period of cone degeneration and that the insulin/mTOR pathway is involved.

A recent report showed that constitutive expression of proinsulin in the rd10 mouse model of retinitis pigmentosa delays photoreceptor death, both of rods and cones[36]. However, proinsulin does not seem to act through the insulin receptor, as mice treated with proinsulin did not develop hyperglycemia. Proinsulin blocks developmental cell death and thus may interfere with the apoptotic pathway in the postnatal retina. Although downstream effectors, such as PI3K/Akt, are regulated by insulin and proinsulin signaling, the relationship between the results of the studies reported here on the effects of insulin and proinsulin remain to be determined.

Macroautophagy, which is controlled by mTOR through its downstream target S6K1, was not detected during cone degeneration, whereas CMA appeared to be activated. Increased LAMP-2A levels at the lysosomal membrane are suggestive of an activation of CMA. In addition, the observations concerning mTOR, HIF-1α and GLUT1 are consistent with starvation and CMA. However, additional experiments are needed to prove that starvation and CMA are indeed occurring and to prove that they are an important contributor to cone death.

The lack of detectable macroautophagy does not rule out the possibility that macroautophagy might occur for a short period of time (for example, 24 h) before the activation of CMA. The data only show that macroautophagy is not the main form of autophagy over an extended period of time, which is consistent with the notion that macroautophagy is a short-term response. The prolonged inhibition of macroautophagy is probably the result of increased S6K1 activity, as seen by increased phosphorylated-S6 levels. S6K1 is positively regulated by mTOR and AMP-activated protein kinase[27], which reads out cellular ATP levels. Therefore, although mTOR may report metabolic problems with respect to glucose uptake and reduce energy-consuming processes and improve glycolysis through HIF-1α, AMP-activated protein kinase may report normal cellular ATP levels and inhibit macroautophagy. This may represent a specific response to the energy requirements of cones.

Notably, most of the glucose taken up by photoreceptors never enters the Krebs cycle[37]. Thus, the shortage of glucose may not cause a shortage of ATP. Lactate, provided by Muller glia, can generate ATP via the Krebs cycle[38]. However, glucose is needed to generate NADPH in the pentose phosphate cycle and NADPH is required for synthesis of phospholipids, the building blocks of cell membranes. Photoreceptors shed a portion of their membranes at the tip of the outer segments on a daily cycle. Because reduced levels of glucose would result in a reduction of membrane synthesis, the rate of outer segment shedding may be higher than the rate of membrane synthesis by cones. Consistent with this, outer segment shortening preceded cell death in these four models, as is also observed in human cases of retinitis pigmentosa[16]. In addition, changes that affect lipid metabolism were also seen in the microarray analysis.

Why does the loss of rods result in cone death in retinitis pigmentosa? The previous hypotheses mentioned above share a commonality in that they can't fully explain the pathology that is found in humans. The rod and cone death kinetics shown here clearly argue against a toxin produced by dying rods as a cause for cone death. If a rod toxin caused cone death, then the onset of cone death should have either coincided with the onset of rod death or should have started shortly thereafter, as this would be the period of peak toxin production. Notably, the lack of a trophic factor produced by healthy rods would agree with the onset of cone death seen in all four models, as one would expect the onset of cone death during the end stages of rod death. However, the progression of cone death and the end phase of rod death make this unlikely to be the sole reason for cone death. In the *Pde6b*$^{-/-}$, *Pde6g*$^{-/-}$ and *Rho*$^{-/-}$ mutants, some of the cones survived for many weeks after completion of the end phase of rod death, demonstrating that they were not dependent on a rod trophic factor. In the P23H model, rods died so slowly during the end phase of rod death that they were still present during the entire period of cone death. Although our data do not provide strong support for a trophic factor hypothesis, neither do they rule it out. Interpretation of the aforementioned lack of consistency of the kinetics of rod and cone death, as might be predicted by the trophic factor model, are further compromised by the fact that the four mouse models that we used are from four different genetic backgrounds. Background differences could result in differences,

including different levels of such a factor, that might account for the observed differences in the progression of cone death.

How could our observations of nutritionally deprived cones explain the dependence of cones on rods? The outer segment–RPE interactions are vital, as the RPE shuttles nutrition and oxygen from the choroidal vasculature to photoreceptors. Roughly 95% of all photoreceptors in mouse and human are rods and approximately 20–30 outer segments contact one RPE cell[39,40]. Thus, only 1–2 of those RPE–outer segment contacts are via cones. During the collapse of the ONL, the remaining cone-RPE interactions are probably perturbed. If these interactions drop below a threshold required for the proper flow of nutrients, the loss of rods might result in a reduced flow of nutrients to cones. In all four mouse models, the onset of cone death occurred when the ONL reached one row of cells. This cell density could therefore represent the critical threshold. Then, while the remaining rods die as a result of a mutation in a rod-specific gene, cone death may begin because of nutrient deprivation. Consistent with this notion, cone death progressed more slowly when the remaining rods died slowly.

This proposed mechanism would also explain why the loss of cones does not lead to rod death[41,42]. Because cones are less than 5% of all photoreceptors in humans and mouse, the critical threshold that perturbs outer segment–RPE interactions would not be reached. Further support for this idea is provided by studies in zebrafish, where the overall ratio of rods to cones is reversed (1 to 8). Additionally, the distribution of rods and cones in zebrafish is uneven, with certain regions being rich in cones and other regions being rich in rods. A recently isolated mutation in a cone-specific gene resulted in rod death, but only in regions of high cone density[43], leading the authors to conclude that cell density is the crucial determinant.

We therefore propose that once a critical threshold of cell density is breached, improper outer segment–RPE interactions result in a reduced flow of nutrients (for example, glucose). This results in reduced outer segment membrane synthesis, which in turn further contributes to a reduced uptake of nutrients from the RPE. Ultimately, prolonged starvation, as suggested by the activation of CMA, leads to cell death. Because starvation can occur slowly over extended periods of time and because the rate may change as a result of fluctuations in nutrient uptake, the slow and irregular demise of cones that is observed in humans may be expected. Therefore, this study not only reveals a previously unknown mechanism of cone death in retinitis pigmentosa that should direct future therapeutic approaches, but also provides an explanation for observations reported in the literature with respect to the death kinetics of rods and cones in mice and humans with different retinitis pigmentosa mutations.

METHODS

Animals. Wild-type mice (C57Bl/6N) and *Pde6b*$^{-/-}$ mice (normally referred to as rd1 or FVB/N) were purchased from Taconic Farms. The *Pde6b*$^{-/-}$ mice have a mutation in the β subunit of cGMP PDE[11]. The PDE-γ knockout (*Pde6g*$^{-/-}$) lacks the γ-subunit of PDE[12]. The rhodopsin knockout (*Rho*$^{-/-}$) lacks the rod-specific opsin gene[12,13]. The P23H mouse carries a transgene that has a substitution mutation in the *Rho* gene (proline 23 is replaced with histidine)[14]. Because this mouse carries a transgene, we crossed the strain back to C57Bl/6N to ensure that none of the progeny would carry two alleles of the transgene. The transgene is specifically expressed in rods[44–46]. The cone-*LacZ* line, which was provided by J. Nathans[47] (Johns Hopkins School of Medicine), carries a transgene that expresses *LacZ* under the control of the human red/green opsin promoter and is expressed in all cones in mouse. All procedures were in compliance with the Association for Research in Vision and Ophthalmology Statement for the Use of Animals.

Affymetrix array analysis. RNA was extracted as described previously[48]. Four retinae were used per RNA sample. A minimum of two arrays were analyzed per time point. The statistical significance of each gene expression profile was determined by a Jonckheere-Terpstra test of the hypothesized cone death–patterned alternative, using exact *P* values calculated by the Harding algorithm[49].

qRT-PCR. qRT-PCR for *Opn1sw* and *Gapdh* was performed as described previously[48]. We used the following primers for the *Lamp2* splice forms: *Lamp2* forward primer (CTG AAG GAA GTG AAT GTC TAC ATG), *Lamp2a* reverse primer (GCT CAT ATC CAG TAT GAT GGC), *Lamp2b* reverse primer (CAG AGT CTG ATA TCC AGC ATA G) and *Lamp2c* reverse primer (GAC AGA CTG ATA ACC AGT ACG). The conditions that we used for all three PCRs were 95° for 3 s, 52° for 15 s and 72° for 25 s (**Figs. 2a** and **7d** represent an average of three measurements corrected for *Gapdh*).

Retinal explant cultures. The retina was dissected free from other ocular tissues in DMEM medium and then incubated (conditions listed in **Supplementary Fig. 5**). The glucose concentrations were 4.5 g L^{-1} for regular DMEM and 1 g L^{-1} for low-glucose DMEM. Leucine was added at 200 μM and fetal calf serum at 10% (vol/vol). Incubation was performed for 4 h and the retinae were fixed and processed for antibody staining as described below.

TUNEL, X-gal histochemistry and *in situ* hybridizations. TUNEL staining, X-gal histochemistry and *in situ* hybridizations were carried out as described previously[48]. To double label cones (**Supplementary Fig. 9** online), we fixed retinae in 2% paraformaldehyde (weight) for 15 min, processed them for the X-gal reaction and then post-fixed them in 4% paraformaldehyde for 15 min. Biotin-PNA was used in an antibody staining procedure and detected with streptavidin-peroxidase (1:500, Roche) by a 3,3′-diaminobenzidine tetrahydrochloride stain (Sigma) according to the manufacturer's instructions. We used the BE950633 and BI202577 ESTs for the red/green opsin and blue opsin probes, respectively. The probe for *Rho* was generated by subcloning the coding sequence (forward primer, 5′-AGC CAT GAA CGG CAC AGA GGG-3′; reverse primer, 5′-CTT AGG CTG GAG CCA CCT GGC T-3′) of the gene into pGEM-T Easy (Promega).

Viral injections. We carried out viral injections as described previously[32]. Mice were injected at embryonic day 10 and harvested at postnatal week 10 (PW10). The GFP-LC3 fusion protein that we used was generated by recombinant PCR with a NotI site at the 5′ of the fusion protein followed by GFP, then LC3, and then an XhoI site at the 3′ of the fusion protein and cloned into pQCXIX as NotI-XhoI fragment (Clonetech, cat# 631515). To create the fusion protein, we used primers for 5′ NotI-GFP (5′-ATG CGG GCC GCC ACC ATG GTG AGC AAG GGC GAG GAG C-3′), 3′ GFP-LC3 (5′-AGG TCT TCT CGG ACG GCA TCT TGT ACA GCT CGT CCA TGC–CGA G-3′), 5′ LC3 (5′-ATG CCG TCC GAG AAG ACC TTC AAG C-3′) and 3′ LC3-XhoI (5′-ATC TCG AGT TAC ACA GCC ATT GCT GTC CCG AAT G-3′).

Rapamycin, streptozotocin and insulin treatments. Rapamycin was diluted to 10 mg ml^{-1} in ethanol. The stock was diluted to 0.015 mg ml^{-1} in drinking water over a period of 2 weeks. We injected 150 μl (12 mg ml^{-1} in 0.1 M citric acid, pH 4.5) of streptozotocin intraperitoneally at postnatal day 21 (P21). Insulin was injected intraperitoneally daily starting at P21. The concentration was increased weekly such that 10 U per kg of body weight were injected the first week, 15 U per kg the second, 20 U per kg the third and 30 U per kg the fourth. In the treatment that lasted for 7 weeks, 30 U per kg were injected for the remaining 3 weeks. Blood glucose levels were measured by collecting a drop of blood from the tail directly onto a test strip from the TrueTrack smart system (CVS Pharmacy). Eye bleeds were avoided because we were assaying cell survival in the retina.

Quantification of cone survival. For procedures, see **Supplementary Figure 10** online.

Whole-mount and section antibody staining. Antibody staining was carried out as previously[32] described, with a few modifications. Triton X-100 was replaced with 0.01% saponin for LAMP-2 staining and phosphate-buffered saline was replaced by tris-buffered saline in every step of the procedure for P-mTOR and P-S6 staining. For primary antibodies, we used mouse antibody to rhodopsin Rho4D2 (1:200)[50], goat antibody to β-galactosidase (1:400, Serotec), rabbit antibody to blue opsin (1:1,000, J. Nathans), rabbit antibody to guanine

nucleotide protein alpha transducin (Gnat1, 1:200, Santa Cruz), rabbit antibody to cleaved caspase3 (1:100, Cell Signaling), rabbit antibody to cleaved LaminA (1:100, Cell Signaling), rabbit antibody to GLUT-1 (1:100, Alpha Diagnostics), rabbit antibody to P-mTOR (1:300, Ser2448, Cell Signaling), rabbit antibody to P-S6 (1:100, Ser235/236, Cell Signaling), rabbit antibody to HIF-1α (1:300, R&D Systems) and rat antibody to LAMP-2 (1:200, clone GL2A7, from the Developmental Studies Hybridoma Bank). We analyzed rod and cone death kinetics in *Pde6b*$^{-/-}$ mice daily from P10–20, weekly from PW3–10 and at PW 12, PW15, PW18 and PW45, in *Pde6g*$^{-/-}$ mice daily from P10–20, weekly from PW3–10 and at PW15, PW25, PW45, in *Rho*$^{-/-}$ mice weekly from PW4–8, and at PW10, PW11, PW17, PW20, PW25, PW27, PW31, PW34, PW37, PW45, PW55 and PW80, and in P23H mutant mice at PW5, PW10, PW16, PW25, PW30, PW35, PW40, PW65, PW70, PW75, PW80 and PW85.

Note: Supplementary information is available on the Nature Neuroscience website.

ACKNOWLEDGMENTS

We thank J. Nathans for the cone-lacZ mouse line and the blue-cone opsin antibody. We are grateful to S. Tsang, M. Naash and J. Lem for the *Pde6b*$^{-/-}$, P23H and *Rho*$^{-/-}$ mice, respectively. The LAMP-2 antibody, developed by B. Granger, was obtained from the Developmental Studies Hybridoma Bank developed under the auspices of the US National Institute of Child Health and Human Development and maintained by the University of Iowa. We thank J. Trimarchi, R. Kanadia, N. Perrimon, J. Zirin, M. Feany and C. Tabin for critical reading of the manuscript. This work was supported by the US National Institutes of Health (RO1 EY014466), Macular Vision Research Foundation, Foundation for Retinal Research, Howard Hughes Medical Institute, Merck and by an EMBO fellowship to C.P.

AUTHOR CONTRIBUTIONS

C.P. conducted the experiments and wrote the manuscript. K.K. performed computational microarray analysis. C.L.C. supervised the project and wrote the manuscript.

Published online at http://www.nature.com/natureneuroscience
Reprints and permissions information is available online at http://npg.nature.com/reprintsandpermissions/

1. Steinberg, R.H. Survival factors in retinal degenerations. *Curr. Opin. Neurobiol.* **4**, 515–524 (1994).
2. Mohand-Said, S. *et al.* Normal retina releases a diffusible factor stimulating cone survival in the retinal degeneration mouse. *Proc. Natl. Acad. Sci. USA* **95**, 8357–8362 (1998).
3. Streichert, L.C., Birnbach, C.D. & Reh, T.A. A diffusible factor from normal retinal cells promotes rod photoreceptor survival in an *in vitro* model of retinitis pigmentosa. *J. Neurobiol.* **39**, 475–490 (1999).
4. Mohand-Said, S. *et al.* Photoreceptor transplants increase host cone survival in the retinal degeneration (rd) mouse. *Ophthalmic Res.* **29**, 290–297 (1997).
5. Mohand-Said, S., Hicks, D., Dreyfus, H. & Sahel, J.A. Selective transplantation of rods delays cone loss in a retinitis pigmentosa model. *Arch. Ophthalmol.* **118**, 807–811 (2000).
6. Leveillard, T. *et al.* Identification and characterization of rod-derived cone viability factor. *Nat. Genet.* **36**, 755–759 (2004).
7. Gupta, N., Brown, K.E. & Milam, A.H. Activated microglia in human retinitis pigmentosa, late-onset retinal degeneration and age-related macular degeneration. *Exp. Eye Res.* **76**, 463–471 (2003).
8. Komeima, K., Rogers, B.S., Lu, L. & Campochiaro, P.A. Antioxidants reduce cone cell death in a model of retinitis pigmentosa. *Proc. Natl. Acad. Sci. USA* **103**, 11300–11305 (2006).
9. Komeima, K., Rogers, B.S. & Campochiaro, P.A. Antioxidants slow photoreceptor cell death in mouse models of retinitis pigmentosa. *J. Cell Physiol.* **213**, 809–815 (2007).
10. Yu, D.Y. & Cringle, S.J. Retinal degeneration and local oxygen metabolism. *Exp. Eye Res.* **80**, 745–751 (2005).
11. Bowes, C. *et al.* Retinal degeneration in the rd mouse is caused by a defect in the beta subunit of rod cGMP-phosphodiesterase. *Nature* **347**, 677–680 (1990).
12. Tsang, S.H. *et al.* Retinal degeneration in mice lacking the gamma subunit of the rod cGMP phosphodiesterase. *Science* **272**, 1026–1029 (1996).
13. Lem, J. *et al.* Morphological, physiological, and biochemical changes in rhodopsin knockout mice. *Proc. Natl. Acad. Sci. USA* **96**, 736–741 (1999).
14. Naash, M.I., Hollyfield, J.G., al-Ubaidi, M.R. & Baehr, W. Simulation of human autosomal dominant retinitis pigmentosa in transgenic mice expressing a mutated murine opsin gene. *Proc. Natl. Acad. Sci. USA* **90**, 5499–5503 (1993).
15. Applebury, M.L. *et al.* The murine cone photoreceptor: a single cone type expresses both S and M opsins with retinal spatial patterning. *Neuron* **27**, 513–523 (2000).
16. John, S.K., Smith, J.E., Aguirre, G.D. & Milam, A.H. Loss of cone molecular markers in rhodopsin-mutant human retinas with retinitis pigmentosa. *Mol. Vis.* **6**, 204–215 (2000).
17. Reiling, J.H. & Sabatini, D.M. Stress and mTORture signaling. *Oncogene* **25**, 6373–6383 (2006).
18. Dekanty, A., Lavista-Llanos, S., Irisarri, M., Oldham, S. & Wappner, P. The insulin-PI3K/TOR pathway induces a HIF-dependent transcriptional response in *Drosophila* by promoting nuclear localization of HIF-alpha/Sima. *J. Cell Sci.* **118**, 5431–5441 (2005).
19. Hudson, C.C. *et al.* Regulation of hypoxia-inducible factor 1alpha expression and function by the mammalian target of rapamycin. *Mol. Cell. Biol.* **22**, 7004–7014 (2002).
20. Treins, C., Giorgetti-Peraldi, S., Murdaca, J., Semenza, G.L. & Van Obberghen, E. Insulin stimulates hypoxia-inducible factor 1 through a phosphatidylinositol 3-kinase/target of rapamycin–dependent signaling pathway. *J. Biol. Chem.* **277**, 27975–27981 (2002).
21. Zhong, H. *et al.* Modulation of hypoxia-inducible factor 1alpha expression by the epidermal growth factor/phosphatidylinositol 3-kinase/PTEN/AKT/FRAP pathway in human prostate cancer cells: implications for tumor angiogenesis and therapeutics. *Cancer Res.* **60**, 1541–1545 (2000).
22. Thomas, G.V. *et al.* Hypoxia-inducible factor determines sensitivity to inhibitors of mTOR in kidney cancer. *Nat. Med.* **12**, 122–127 (2006).
23. Wang, G.L., Jiang, B.H., Rue, E.A. & Semenza, G.L. Hypoxia-inducible factor 1 is a basic helix-loop-helix-PAS heterodimer regulated by cellular O2 tension. *Proc. Natl. Acad. Sci. USA* **92**, 5510–5514 (1995).
24. Ebert, B.L., Firth, J.D. & Ratcliffe, P.J. Hypoxia and mitochondrial inhibitors regulate expression of glucose transporter 1 via distinct Cis-acting sequences. *J. Biol. Chem.* **270**, 29083–29089 (1995).
25. Massey, A., Kiffin, R. & Cuervo, A.M. Pathophysiology of chaperone-mediated autophagy. *Int. J. Biochem. Cell Biol.* **36**, 2420–2434 (2004).
26. Finn, P.F. & Dice, J.F. Proteolytic and lipolytic responses to starvation. *Nutrition* **22**, 830–844 (2006).
27. Codogno, P. & Meijer, A.J. Autophagy and signaling: their role in cell survival and cell death. *Cell Death Differ.* **12** Suppl 2: 1509–1518 (2005).
28. Dice, J.F. Chaperone-mediated autophagy. *Autophagy* **3**, 295–299 (2007).
29. Kunchithapautham, K. & Rohrer, B. Apoptosis and autophagy in photoreceptors exposed to oxidative stress. *Autophagy* **3**, 433–441 (2007).
30. Kabeya, Y. *et al.* LC3, a mammalian homologue of yeast Apg8p, is localized in autophagosome membranes after processing. *EMBO J.* **19**, 5720–5728 (2000).
31. Mizushima, N., Yamamoto, A., Matsui, M., Yoshimori, T. & Ohsumi, Y. *In vivo* analysis of autophagy in response to nutrient starvation using transgenic mice expressing a fluorescent autophagosome marker. *Mol. Biol. Cell* **15**, 1101–1111 (2004).
32. Punzo, C. & Cepko, C.L. Ultrasound-guided in utero injections allow studies of the development and function of the eye. *Dev. Dyn.* **237**, 1034–1042 (2008).
33. Cuervo, A.M. & Dice, J.F. Regulation of lamp2a levels in the lysosomal membrane. *Traffic* **1**, 570–583 (2000).
34. Kiffin, R., Christian, C., Knecht, E. & Cuervo, A.M. Activation of chaperone-mediated autophagy during oxidative stress. *Mol. Biol. Cell* **15**, 4829–4840 (2004).
35. Cuervo, A.M. & Dice, J.F. Unique properties of lamp2a compared to other lamp2 isoforms. *J. Cell Sci.* **113**, 4441–4450 (2000).
36. Corrochano, S. *et al.* Attenuation of vision loss and delay in apoptosis of photoreceptors induced by proinsulin in a mouse model of retinitis pigmentosa. *Invest. Ophthalmol. Vis. Sci.* **49**, 4188–4194 (2008).
37. Poitry-Yamate, C.L., Poitry, S. & Tsacopoulos, M. Lactate released by Muller glial cells is metabolized by photoreceptors from mammalian retina. *J. Neurosci.* **15**, 5179–5191 (1995).
38. Tsacopoulos, M., Poitry-Yamate, C.L., MacLeish, P.R. & Poitry, S. Trafficking of molecules and metabolic signals in the retina. *Prog. Retin. Eye Res.* **17**, 429–442 (1998).
39. Snodderly, D.M., Sandstrom, M.M., Leung, I.Y., Zucker, C.L. & Neuringer, M. Retinal pigment epithelial cell distribution in central retina of rhesus monkeys. *Invest. Ophthalmol. Vis. Sci.* **43**, 2815–2818 (2002).
40. Young, R.W. The renewal of rod and cone outer segments in the rhesus monkey. *J. Cell Biol.* **49**, 303–318 (1971).
41. Biel, M. *et al.* Selective loss of cone function in mice lacking the cyclic nucleotide–gated channel CNG3. *Proc. Natl. Acad. Sci. USA* **96**, 7553–7557 (1999).
42. Yang, R.B. *et al.* Disruption of a retinal guanylyl cyclase gene leads to cone-specific dystrophy and paradoxical rod behavior. *J. Neurosci.* **19**, 5889–5897 (1999).
43. Stearns, G., Evangelista, M., Fadool, J.M. & Brockerhoff, S.E. A mutation in the cone-specific *pde6* gene causes rapid cone photoreceptor degeneration in zebrafish. *J. Neurosci.* **27**, 13866–13874 (2007).
44. Gouras, P., Kjeldbye, H. & Zack, D.J. Reporter gene expression in cones in transgenic mice carrying bovine rhodopsin promoter/*LacZ* transgenes. *Vis. Neurosci.* **11**, 1227–1231 (1994).
45. Woodford, B.J., Chen, J. & Simon, M.I. Expression of rhodopsin promoter transgene product in both rods and cones. *Exp. Eye Res.* **58**, 631–635 (1994).
46. al-Ubaidi, M.R. *et al.* Mouse opsin. Gene structure and molecular basis of multiple transcripts. *J. Biol. Chem.* **265**, 20563–20569 (1990).
47. Wang, Y. *et al.* A locus control region adjacent to the human red and green visual pigment genes. *Neuron* **9**, 429–440 (1992).
48. Punzo, C. & Cepko, C. Cellular responses to photoreceptor death in the rd1 mouse model of retinal degeneration. *Invest. Ophthalmol. Vis. Sci.* **48**, 849–857 (2007).
49. Harding, E.F. An efficient, minimal-storage procedure for calculating the Mann-Whitney U, generalized U and similar distributions. *Appl. Stat.* **33**, 1–6 (1984).
50. Molday, R.S. & MacKenzie, D. Monoclonal antibodies to rhodopsin: characterization, cross-reactivity and application as structural probes. *Biochemistry* **22**, 653–660 (1983).

Stimulation of the insulin/mTOR pathway delays cone death in a mouse model of Retinitis Pigmentosa.
Claudio Punzo, Karl Kornacker & Constance L. Cepko.

Supplementary Material

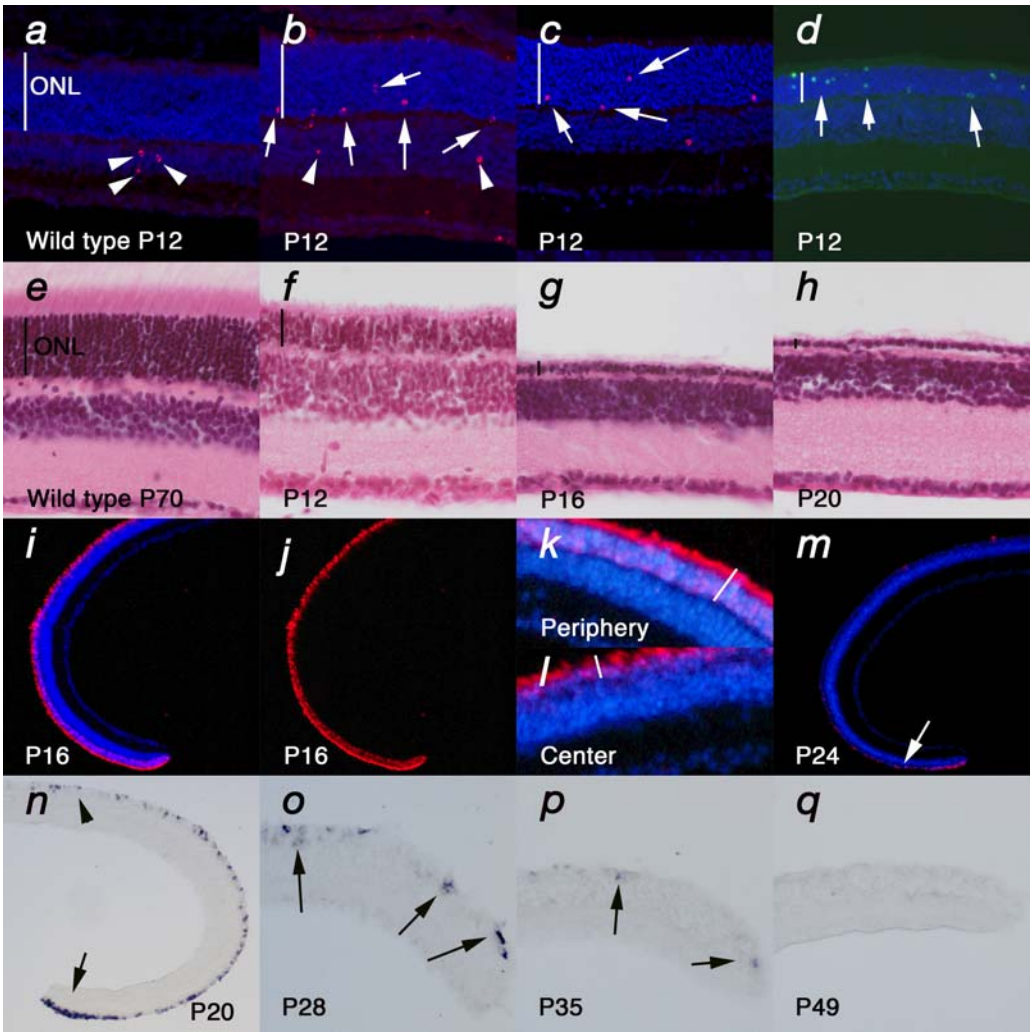

Supplementary Figure 1

Figure 1: Rod death kinetics in the PDE-$\gamma^{-/-}$. All panels show PDE-$\gamma^{-/-}$ except (**a**, **e**) which show wild type. (**a–d**) Onset of rod death seen by Cleaved Caspase3 (**a**, **b**). At this age misplaced and excess cells in the INL are still dying as seen in a wild-type control (**a**) (arrowheads: red signal) while in the mutant cells start to die also in the ONL where the rods reside (**b**) (arrows: red signal). The onset of rod cell death can also be seen by the cleaved nuclear envelope protein LaminA (**c**) (arrows; red signal) as well as TUNEL (**d**) (arrows: green signal; blue in **a–d** shows nuclear DAPI staining). Progression of rod death determined by the reduction of the ONL as seen by HE staining (**e–h**). (**i–q**) End phase of rod death assessed by section analysis of progressively older animals. (**i–m**) Rods were visualized by immunofluorescence with an antibody directed against rhodopsin or by *in situ* hybridizations for *rhodopsin* (**n–q**). (**i**, **j**) Retinal section at P16 showing peripheral to central region. (**i**) Same picture as in (**j**) with nuclear DAPI stain. (**k**, **l**) Higher magnification of section in (**i**) showing peripheral (**k**) and central (**l**) region. As rods die in a central to peripheral manner more rods are present in the center than in the periphery. By P20 the ONL is reduced to 1 row of cells and rods are found mainly in the periphery (compare arrow (periphery) in (**n**) to arrowhead (central). The remaining rods in the PDE-$\gamma^{-/-}$ die over a time of 4 weeks (**n–q**) as seen on sections. By P49 (**q**) all rods had died in this mutant (**o–q**: periphery). Age (in postnatal days (P)) is indicated in the panels. Vertical bar in (**a–h**, **k**, **l**) indicates thickness of the ONL. Data for PDE-$\beta^{-/-}$ are not shown as they are comparable to the PDE-$\gamma^{-/-}$.

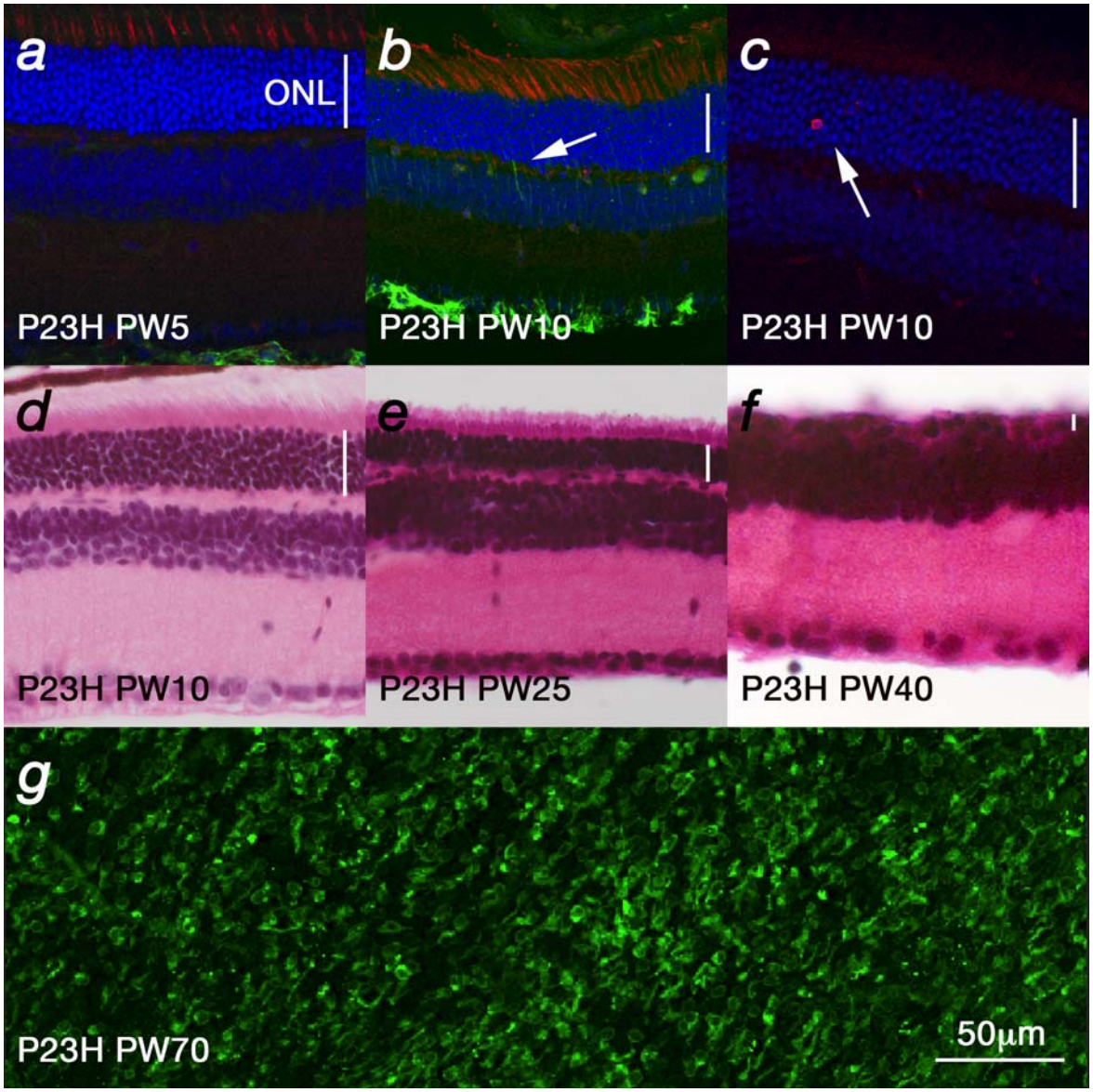

Supplementary Figure 2

Figure 2: Rod death kinetics in the P23H mutant. (**a–c**) Onset of rod death. As rod death progresses much slower in this mutant we also used the upregulation of *glial fibrillary acidic protein* (GFAP) in Muller glia, which has been described as a hallmark of retinal degeneration to determine the onset of rod death. As seen by antibody staining against GFAP *(***a**, **b***)* rod death starts around PW10 (**b**). At PW5 GFAP is only found in the ganglion cell layer where it is normally expressed in astrocytes. Consistent with the upregulation of GFAP at PW10, cells positive for cleaved nuclear envelope protein LaminA *(***c**) are also detected (arrow: red signal). However only few cells are seen per section due to the slow progression of rod death. (**d–f**) Progression of rod death determined by the reduction of the ONL as seen by HE staining. (**g**) End phase of rod death assessed by immunofluorescence with an antibody directed against rhodopsin. Although the ONL is reduced to one row of cells by PW35 no end point of rod death was determined. Rods continue to die slow and even by PW70 many rods are still present (**g**). Interestingly, most of those rods at that age are confined to the ventral regions of the retina (see also **Supplementary Fig. 3**). Age (in postnatal weeks (PW)) is indicated in the panels. Vertical bar in (**a–f**) indicates thickness of the ONL.

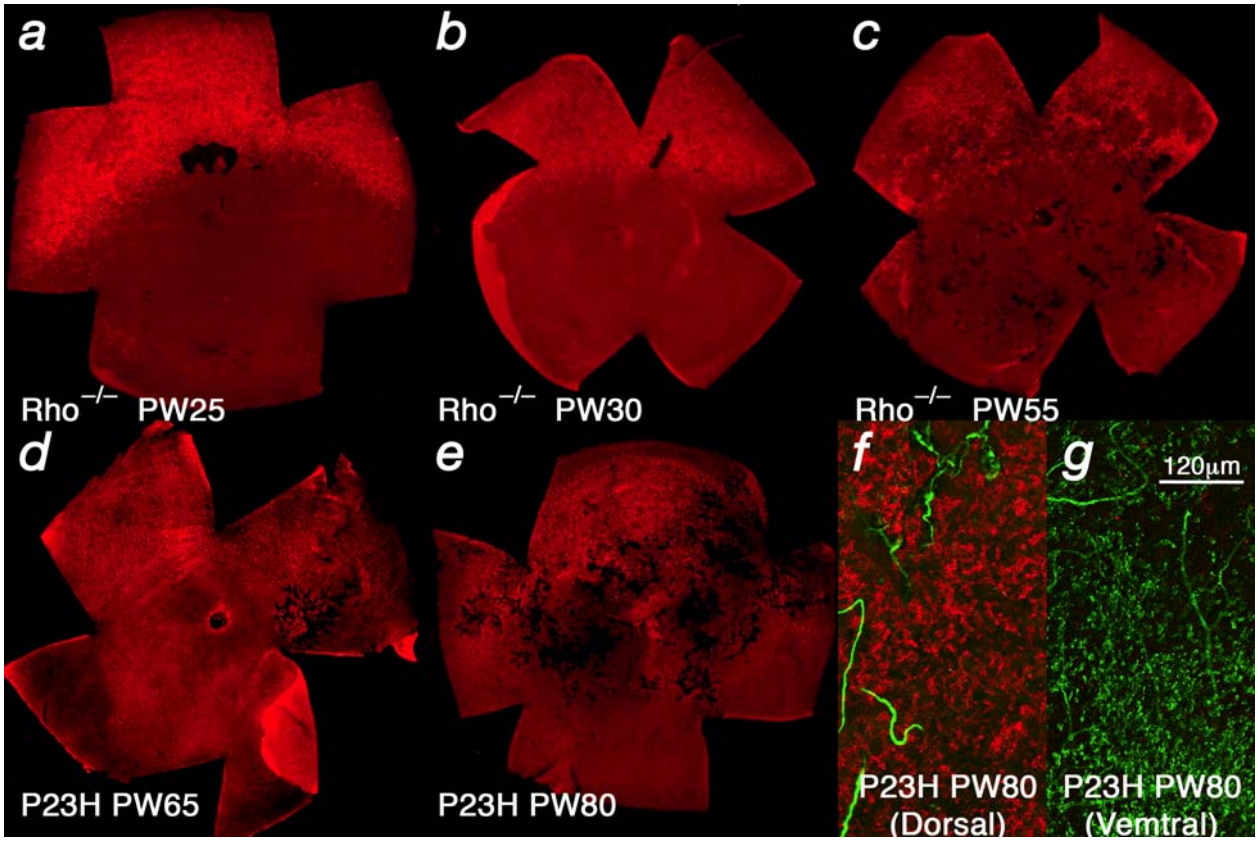

Supplementary Figure 3

Figure 3: Dorsal cone death kinetics seen by the expression of red/green opsin. (**a–c**) Loss of dorsal cones in the $Rho^{-/-}$ mutant over time as seen by the reduced expression of red-green opsin. (**d**, **e**) Loss of dorsal cones in the P23H mutant over time. (**f**, **g**) Higher magnification of a double staining with an antibody against red/green opsin (red signal) and rhodopsin (green signal) showing that most rods that survive up to PW80 are in the ventral regions (**g**) of the retina whereas the red/green expressing cones are dorsally (**f**).

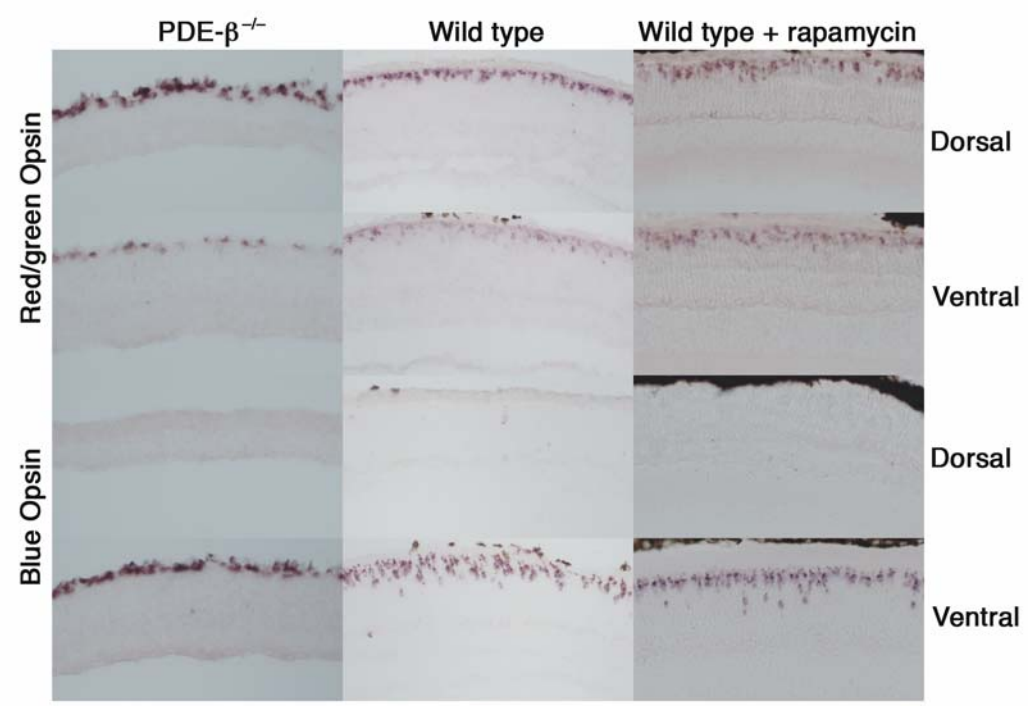

Supplementary Figure 4

Figure 4: Red/green opsin expression was affected on a protein level. *In situ* hybridization for red/green opsin (first two rows) or blue opsin (third and fourth row) mRNA on retinal sections. mRNA levels for red/green opsin were comparable between ventral regions of PDE-$\beta^{-/-}$ mutant animals (first column), wild type animals treated with rapamycin (last column) or untreated wild type animals (second column). mRNA levels of blue opsin remained also unaffected.

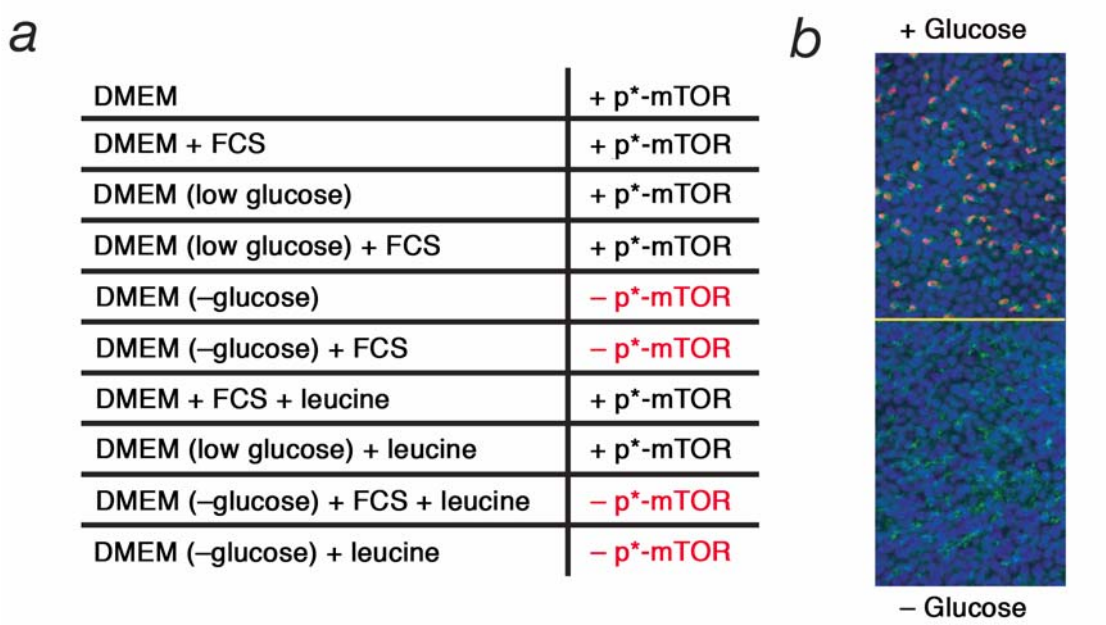

Supplementary Figure 5

Figure 5: p*-mTOR levels were dependent of the presence of glucose. Different media conditions were tested (**a**) during 4 hours retinal explant culture. Retinae were then fixed and stained for p*-mTOR (red signal), PNA (green signal) and DAPI (blue signal) and then flat mounted and imaged (**b**). p*-mTOR was only detected when glucose was present in the media (**a**).

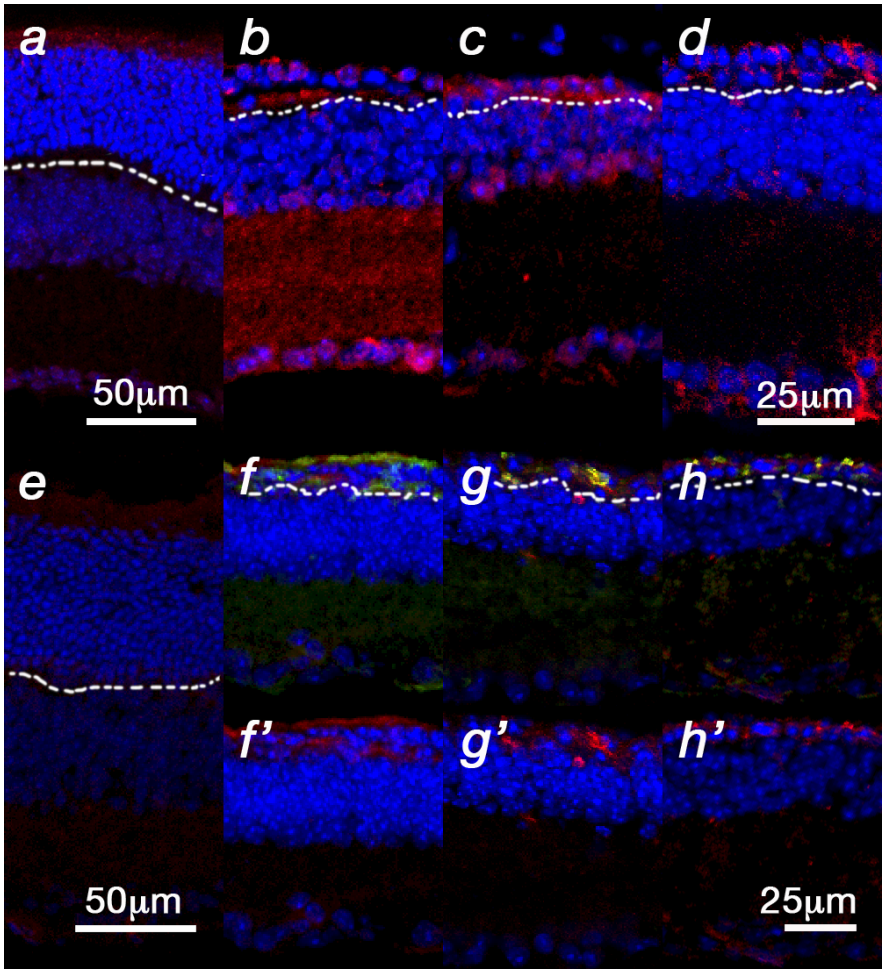

Supplementary Figure 6

Figure 6: Upregulation of Hif-1α and GLUT1 in cones. All panels show immunofluorescent stainings of retinal sections. Blue shows nuclear DAPI staining and green shows cones marked with PNA. (**a–d**) Staining for HIF-1α (red signal). (**a**) Wild type at PW10. (**b**) PDE-$\gamma^{-/-}$ at PW5. (**c**) Rho$^{-/-}$ at PW20. (**d**) P23H mutant at PW70. (**e–h**) Increased expression of GLUT1 in cones during degeneration (red signal). (**e**) Wild type at PW10. (**f**) PDE-$\gamma^{-/-}$ at PW5 with PNA overlap. (**f'**) Same image as (**f**) without PNA. (**g**) Rho$^{-/-}$ at PW20. (**g'**) Same image as (**g**) without PNA. (**h**) P23H mutant at PW70. (**h'**) Same image as (**h**) without PNA. White dotted line marks border between the ONL and INL.

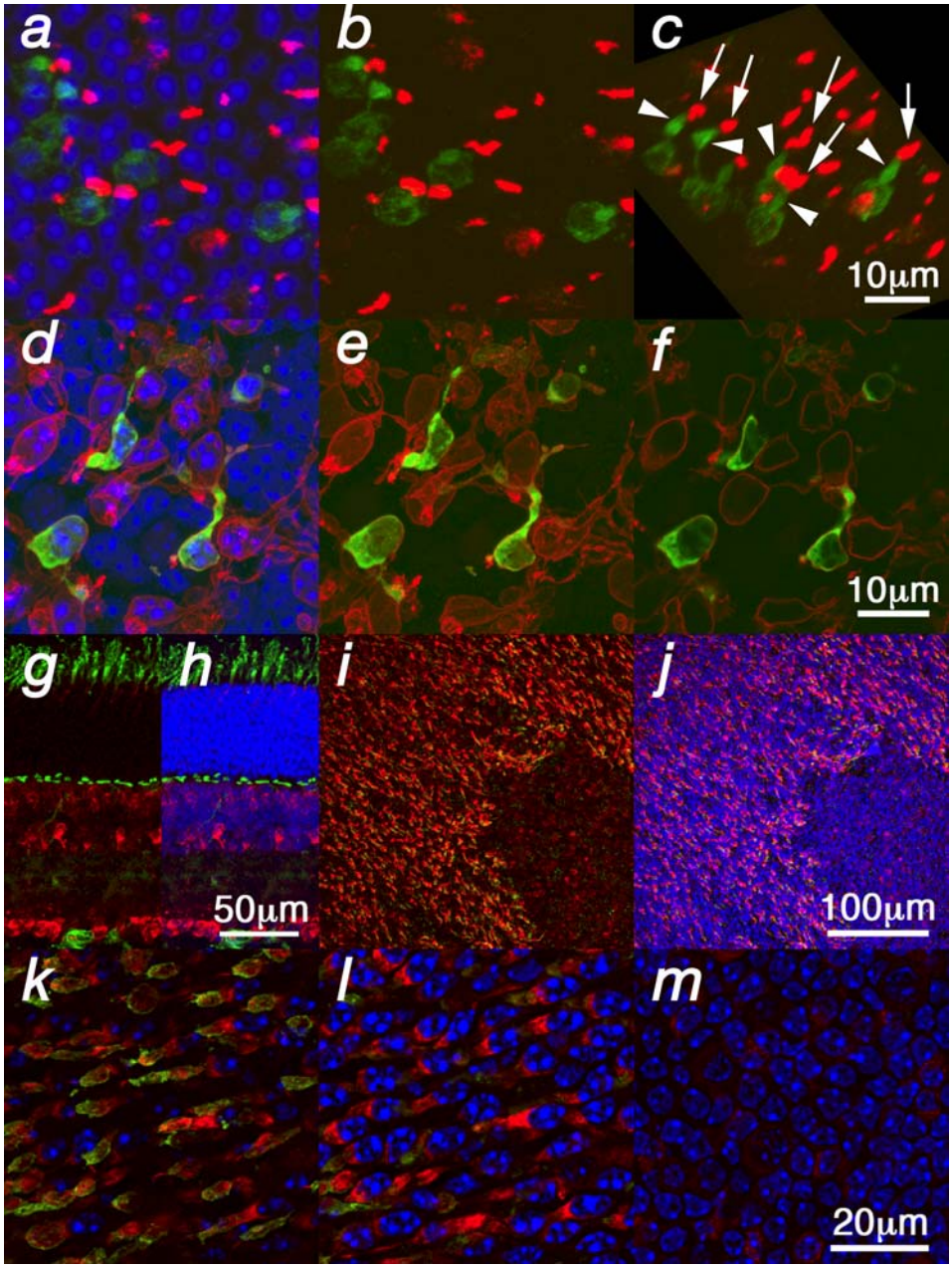

Supplementary Figure 7

Figure 7: Macroautophagy in PDE-β$^{-/-}$**.** (**a–f**) Viral infections expressed a fusion protein between GFP and LC3 in wild type (**a–c**) and PDE-β$^{-/-}$ (**d–f**) retinae. Green signal shows expression of fusion protein, red signal shows red/green opsin expression and blue signal show nuclear DAPI staining. (**a–f**) Retinal flat mounts at PW10 showed uniform expression of the GFP fusion protein in cones without the formation of vesicular structures in wild type and mutant retinae. (**a**) DAPI overlap of (**b**). (**c**) 3D reconstruction of (**b**). Cone outer segments as seen by red/green opsin (arrow) were attached to the cone inner segment (arrowhead) seen as GFP signal. (**d**) DAPI overlap of (**e**). (**f**) Single confocal section showing cytoplasmic GFP and membrane bound red green opsin (see also **Supplementary Fig. 2**). (**g–m**) Levels of phosphorylated S6 (p*-S6) (red signal) in wild type (**g**, **h**) and mutant (**i–m**) cones. (**g**) Low levels of p*-S6 were seen in wild type cones but not in cone OSs. (**h**) DAPI overlap of (**g**). (**i**, **j**) Strong uniform expression in cones was seen the PDE-β mutant shortly after the phase of major rod death (PW3). Area in lower right corner shows region where cones had started to die. (**j**) DAPI overlap of (**i**). (**k–l**) Higher magnification at PW5 showing same field at three different confocal depths. (**k**) At the plane of the cone segments high levels of p*-S6 was seen in cones when compared to segments of wild type cones. (**l**) Strong staining is also seen at the plane of the cone nuclei suggesting a uniform cytoplasmic distribution. (**m**) At the plane of the inner nuclear layer levels of p*-S6 were much lower than in cones.

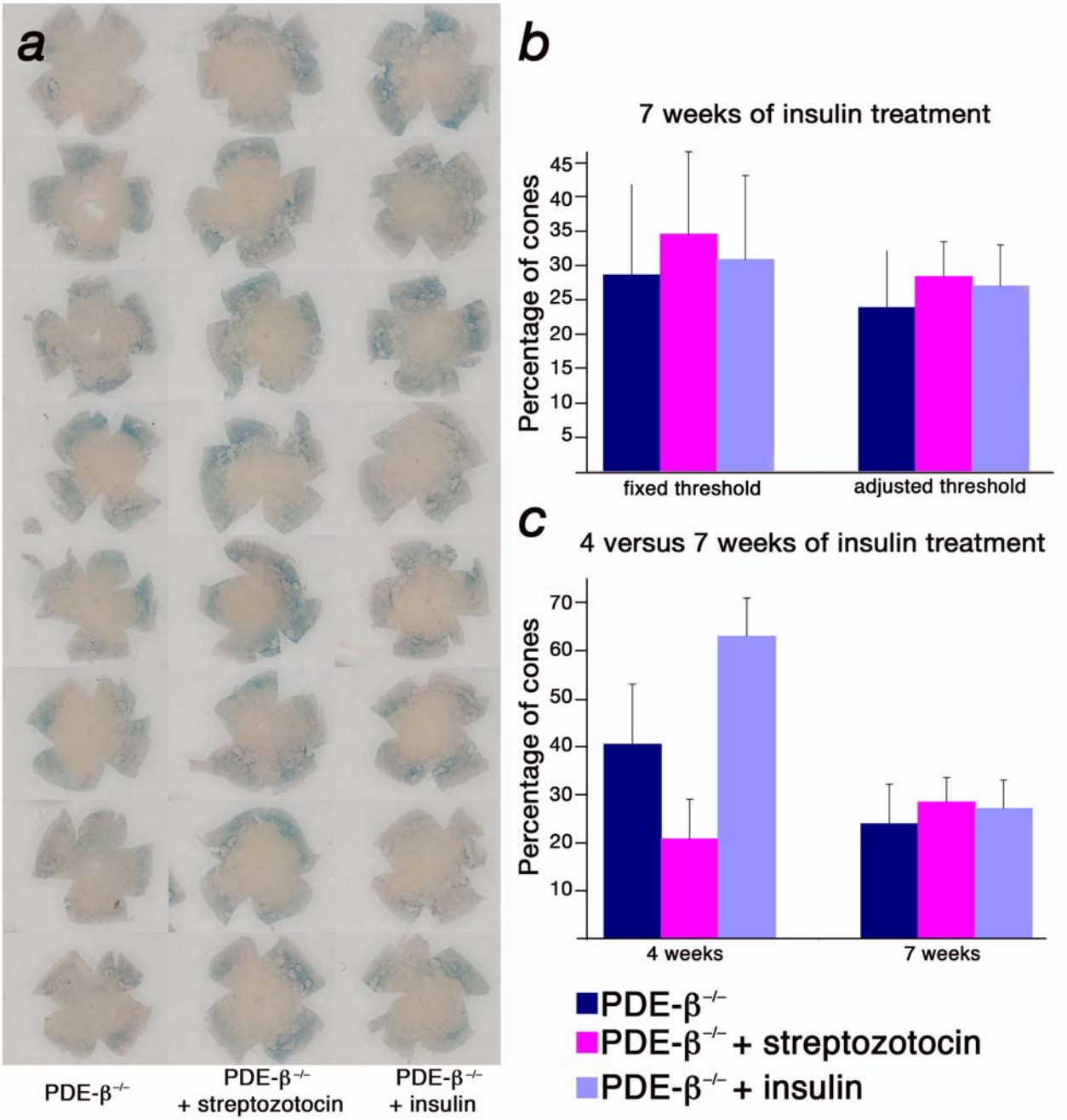

Supplementary Figure 8

Figure 8: Assessment of cone survival after prolonged Insulin treatment. (**a**) Composite of retinae after lacZ staining. First column shows untreated PDE-$\beta^{-/-}$ mice at PW10. Second column shows retinae of PDE-$\beta^{-/-}$ mice at PW10 that received a single injection of streptozotocin at PW3. Third column shows retinae of PDE-$\beta^{-/-}$ mice at PW10 that received daily injections of insulin starting at PW3. (**b**) Shows quantification of cone survival by the two methods described in **Supplementary Fig. 10**. There was no significant difference in cone survival between treated and untreated mice at PW10. (**c**) Shows comparison between the 4 and 7 weeks treatment. Error bars in (**b**, **c**) show standard deviation.

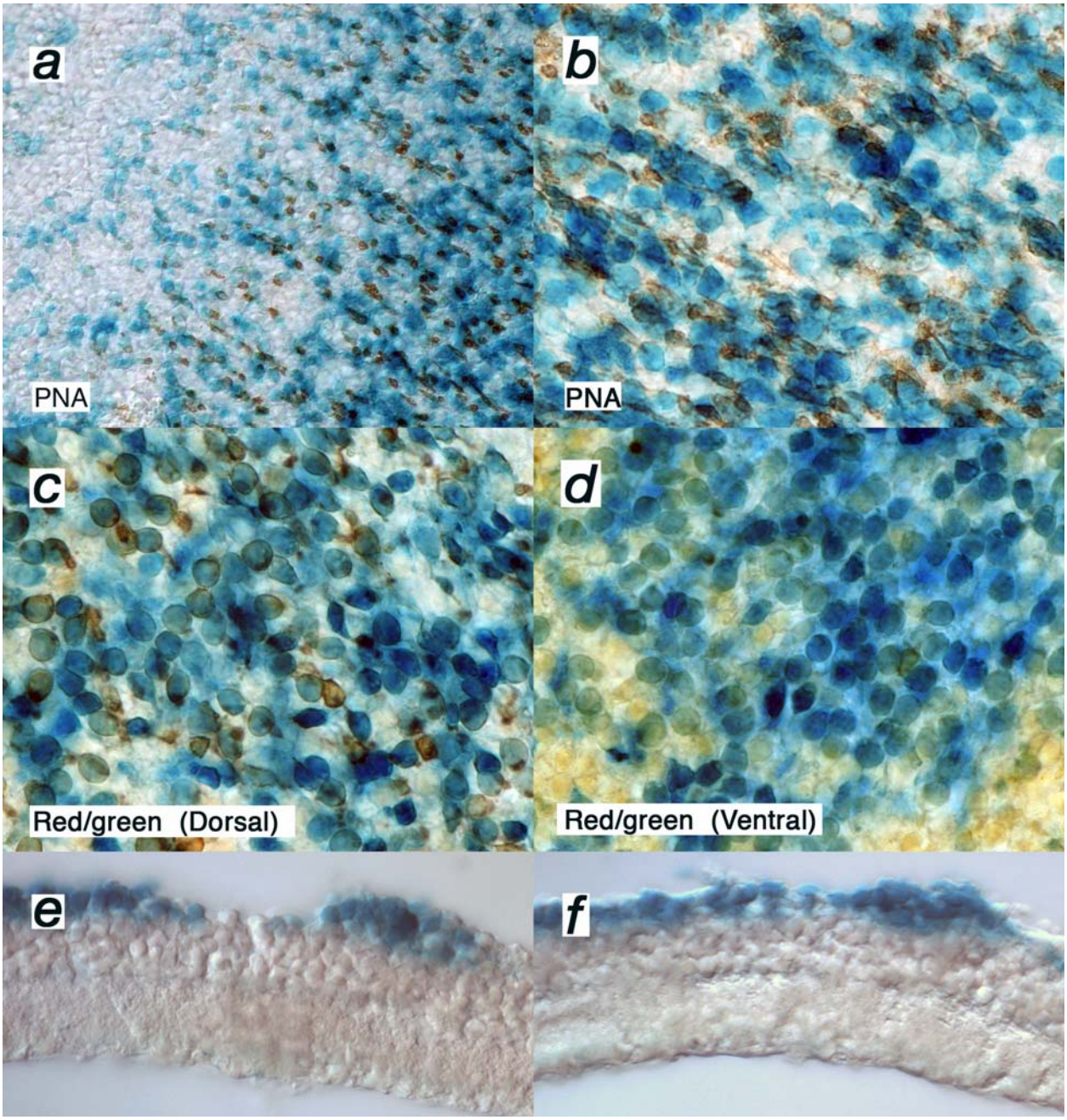

Supplementary Figure 9

Figure 9: Cone-lacZ transgene in the PDE-β mutant at 7 weeks of age. (**a**, **b**) Double labeling of cones with PNA (brown signal) and lacZ staining (blue signal). More cones were labelled by lacZ than by PNA. Since PNA marks an extra cellular matrix protein of the OS, once the OSs were reduced, PNA became a less reliable marker. (**c**, **d**) Double labeling of cones by α-red/green opsin (brown signal) and lacZ staining (X-gal; blue signal) in the dorsal (**c**) and ventral (**d**) retina. Red/green opsin levels decreased ventrally during degeneration which makes this marker not suitable to detect cones across the retina. (**e**, **f**) Sections of retina stained for lacZ showing the signal in cones on top of the inner nuclear layer.

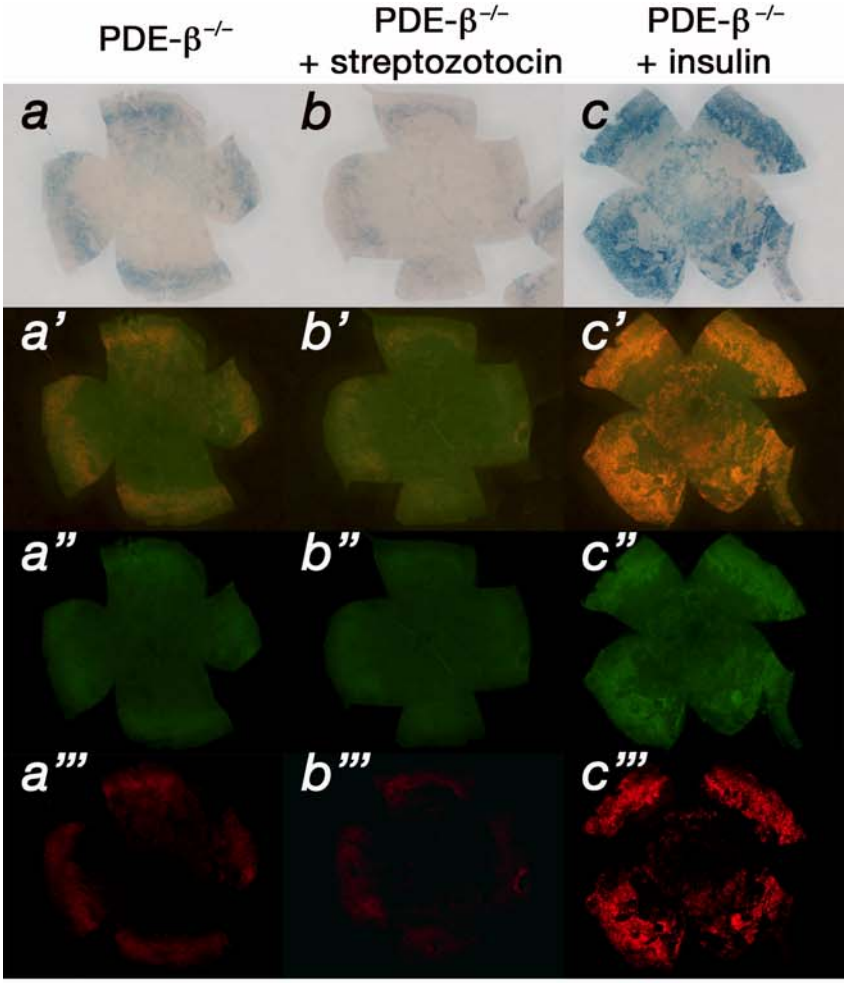

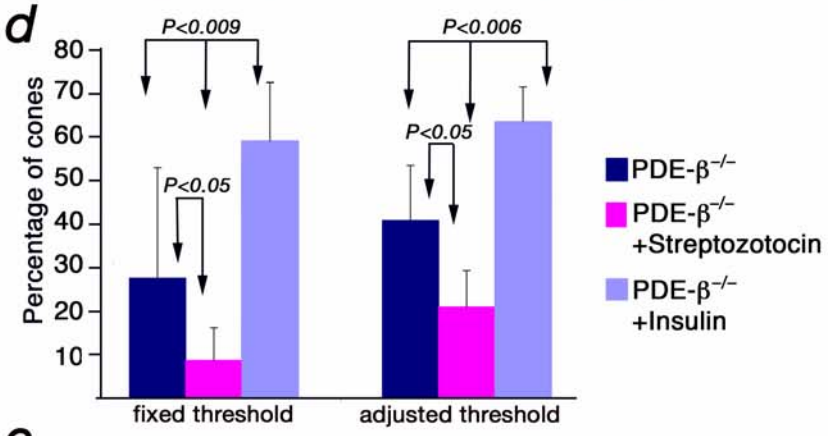

e

PDE-β−/−	PDE-β−/− + streptozotocin	PDE-β−/− + insulin	PDE-β−/−	PDE-β−/− + streptozotocin	PDE-β−/− + insulin
74.99	3.02	54.33	53.27	15.22	59.52
8.47	0.89	68.71	26.81	11.34	68.71
27.89	10.67	47.74	43.04	26.29	58.84
13.68	22.34	67.2	34.33	36.09	67.2
60.97	7.89	74.02	63.97	15.88	72.69
4.12	4.01	50.55	24.88	16.96	55.25
17.01	1.98	32.24	39.12	12.31	47.32
8.05	9.08	67.68	33.87	22.69	67.68
	20.92			32.47	
	2.34			14.72	
	fixed threshold			adjusted threshold	

Supplementary Figure 10

Figure 10: Method to calculate cone survival. The colors of the bright light image were inverted and processed with Imaris software (Bitplane Inc) to calculate the percentage of blue surface area versus the total retinal surface area. A minimum of 8 retinae per treatment, and for the control, were analyzed. P-values were calculated by the student's t-test. The cone lacZ transgene was chosen over PNA as a cone marker since the transgene labels cones more persistently (see **Supplementary Fig. 9** online). (**a–c**) Show retinal flat mounts stained for lacZ (see Fig. 8). (**a**) Untreated control PDE-$\beta^{-/-}$ mouse at PW7. (**b**) PDE-$\beta^{-/-}$ mouse at PW7 treated with one injection of Streptozotocin at PW3. (**c**) PDE-$\beta^{-/-}$ mouse at PW7 treated for 4 weeks with daily injections of insulin starting at PW3. (**a'–c'**) Show inverted color images of corresponding panels (**a–c**). (**a''–c''**) Show only green channels whereas (**a'''–c'''**) show only red channels of (**a'–c'**). (**d**) Quantification of cone survival by calculating the surface area of red that co-localizes with green. Two different methods were employed, a fixed threshold and an adjusted threshold. The fixed threshold was determined by adjusting the lower intensity of the red channel in the image with the most intense lacZ staining (most intense red channel) to reflect the pattern of the lacZ staining. The same threshold for the red channel was then applied to all other images. As this method would under represent cone survival in mice that were not treated with insulin due to the lesser intense lacZ staining a second method was employed. For each image the lower intensity of the red channel was adjusted individually to match the blue pattern of the lacZ staining avoiding the problem of the difference in lacZ intensity. The increased intensity of lacZ in the insulin treated mice could be due to healthier cones that either have an increased transcription/translation or decreased protein degradation. Error bars show standard deviation. (**e**) Shows the actual calculated values in percentage of cone survival for all retinae. Values are shown for the untreated mice, the Streptozotocin treated mice and the insulin treated mice. Values for both types of calculations are shown, for the fixed threshold and adjusted threshold.

Supplementary Table 1: Genes that cross validated in the array study. The 230 genes that cross validated in all 4 models and had fold change >2 at the onset of cone death when compared to the other three time points and had statistically significant changes. The fold change is indicated as $\log_2$. (AVG: Average of fold change from the 4 mutants; C0: Onset of cone death; R: peak of rod death; C1 & C2: first and second time point during cone death respectively, see also **Fig. 4a**)

Affymetrix ID	Gene Symbol	AVG_C0/R	AVG_C0/C1	AVG_C0/C2
1425337_at	Slc12a5	5.42	3.64	4.41
1432646_a_at	EG640370	4.46	3.22	3.83
1425833_a_at	Hpca	4.19	3.12	3.90
1425227_a_at	ATP6V0A1	3.93	2.49	3.41
1425405_a_at	ADAR	3.83	3.28	3.65
1426562_a_at	Olfm1	3.69	3.06	3.03
1415824_at	SCD2	3.66	2.23	2.99
1429385_at	Wdr68	3.54	3.67	3.88
1427754_a_at	DNM1	3.54	2.19	3.01
1420833_at	VAMP2	3.46	2.15	3.36
1454735_at	Odf2	3.45	2.47	2.98
1431107_at	Stk35	3.39	2.45	3.40
1454106_a_at	Cxxc1	3.39	2.72	3.58
1421255_a_at	Cabp1	3.39	2.00	1.98
1421780_a_at	Cabp5	3.36	2.21	2.28
1425338_at	PLCB4	3.33	2.58	2.49
1421349_x_at	Cend1	3.31	2.09	2.56
1425711_a_at	AKT1	3.27	2.23	3.28
1425457_a_at	GRB10	3.23	2.62	3.19
1451056_at	PSMD7	3.23	2.37	2.22
1448541_at	Kns2	3.23	2.27	3.04
1425659_at	Tom1l2	3.21	2.54	3.36
1448997_at	Pscd1	3.18	2.67	3.01
1442138_at	Gpr62	3.14	1.93	1.98
1426115_a_at	Kcnj9	3.13	2.87	2.69
1450202_at	GRIN1	3.13	2.39	2.94
1428157_at	GNG2	3.12	2.95	3.22
1424359_at	OPLAH	3.08	1.42	1.75
1418174_at	Dbp	3.05	1.99	2.12
1426975_at	OS-9	2.97	2.63	3.11
1435276_a_at	Dgcr2	2.96	2.32	2.73
1449936_at	KIAA1467	2.94	1.87	2.30
1455410_at	Faim2	2.93	1.47	1.76
1453127_at	PPM1J	2.93	2.16	2.38
1435770_at	Txndc13	2.93	2.37	2.61
1457914_at	unknown	2.88	2.86	2.91
1458163_at	BC066028	2.86	2.10	1.89
1433714_at	SULT4A1	2.85	1.82	1.79
1436713_s_at	Gtl2	2.84	2.09	2.52
1422756_at	SLC32A1	2.83	2.05	1.91
1452688_at	Prpf39	2.80	2.58	3.19
1421391_at	VIPR2	2.79	2.10	2.18

1446071_at	Steap2	2.78	1.86	2.02
1454891_at	CDS2	2.77	2.09	2.61
1421862_a_at	Vamp1	2.76	1.96	2.46
1440358_at	ARHGEF15	2.74	2.38	2.29
1431355_s_at	TRPM7	2.72	2.60	2.52
1422793_at	PAFAH1B2	2.72	2.25	2.78
1453199_at	Acbd6	2.71	2.09	2.23
1449615_s_at	Hdlbp	2.69	2.64	3.06
1432329_a_at	MATK	2.69	2.18	2.36
1459826_at	Kcnq2	2.68	2.37	2.59
1438205_at	C11ORF2	2.67	2.02	2.57
1426467_s_at	C1ORF123	2.63	2.35	2.74
1429761_at	Rtn1	2.62	2.39	2.27
1420148_at	SLC6A6	2.61	2.41	2.95
1426888_at	EHMT2	2.61	2.55	2.68
1451989_a_at	Mapre2	2.59	1.80	1.81
1450512_at	Ntn4	2.58	2.25	2.12
1415795_at	Spin	2.57	2.49	2.59
1434467_at	Atcay	2.57	2.13	2.21
1426738_at	DGKZ	2.56	1.66	1.90
1419278_at	USP48	2.54	2.08	2.12
1417455_at	TGFB3	2.52	2.19	2.04
1427478_at	USP12	2.50	2.74	2.99
1437319_at	Unc13c	2.48	1.67	1.54
1427004_at	Fbxo2	2.47	1.68	1.55
1450177_at	NGFR	2.46	2.26	2.19
1415845_at	Syt4	2.46	1.78	1.82
1428717_at	Scrn1	2.45	2.11	2.11
1439160_at	4732496O08Rik	2.44	2.27	2.46
1450686_at	Pon2	2.43	1.93	1.68
1415803_at	CX3CL1	2.43	1.33	1.83
1421189_at	GABRB3	2.43	1.84	2.49
1416936_at	Aatk	2.42	1.67	1.84
1416190_a_at	Sec61a1	2.42	2.29	2.96
1452357_at	5-Sep	2.42	1.69	1.77
1450311_at	SLC8A3	2.41	2.10	2.51
1460384_a_at	Arid4b	2.37	1.91	2.19
1434563_at	Rps6kc1	2.37	2.26	2.27
1450080_at	Cxx1c	2.37	1.46	1.69
1444552_at	KIAA0240	2.36	2.28	2.28
1450055_at	Vsnl1	2.35	1.51	1.47
1448498_at	RPS6KA4	2.35	1.69	1.65
1424045_at	C6ORF35	2.33	2.04	2.52
1460321_at	Cntn4	2.32	1.75	1.91
1420387_at	Mpv17	2.32	2.06	2.12
1422694_at	Ttyh1	2.31	1.93	1.94
1433583_at	Zfp365	2.31	2.00	1.90
1431229_at	Ipw	2.30	1.87	1.76
1451975_at	MGC12966	2.30	2.26	1.71
1419399_at	MTTP	2.30	1.95	1.71
1433477_at	Abr	2.28	1.73	1.72

1426114_at	Hnrpab	2.27	2.16	2.03
1424500_at	Utp6	2.26	2.47	2.45
1417658_at	Tbrg4	2.26	1.96	1.74
1457744_at	Ddx46	2.25	2.01	2.25
L09192_3_at	Pcx	2.25	1.59	1.62
1421914_s_at	Mrpl19	2.24	1.79	1.90
1437091_at	Accn4	2.23	1.71	1.74
1426552_a_at	Bcl11a	2.23	1.68	1.81
1435045_s_at	MAPK8IP2	2.22	1.26	1.36
1439036_a_at	ATP1B1	2.22	1.60	1.62
1448581_at	Zfp346	2.21	2.01	2.25
1425846_a_at	Caln1	2.21	1.72	1.70
1416087_at	Ap1s1	2.20	1.37	1.74
1442622_at	STRBP	2.20	2.04	1.98
1437772_s_at	FUCA1	2.20	2.02	2.05
1419428_a_at	GAA	2.17	1.59	1.52
1415687_a_at	PSAP	2.17	1.59	1.71
1415908_at	Tspyl1	2.16	1.35	1.67
1424882_a_at	Nt5dc2	2.14	1.92	2.10
1449406_at	Cyhr1	2.13	2.27	2.76
1448605_at	RHOC	2.13	1.98	2.41
1425615_a_at	PCK2	2.12	1.58	1.54
1435532_at	FAM80B	2.12	1.69	2.01
1436343_at	Chd4	2.10	1.74	1.94
1435281_at	CPT1C	2.10	1.68	1.64
1451290_at	Map1lc3a	2.10	1.69	2.06
1417388_at	Bex2	2.10	1.66	1.48
1438671_at	PPP2R2C	2.10	1.40	1.50
1419812_s_at	Ccdc56	2.08	1.70	1.75
1425551_at	HIP1R	2.08	2.01	1.89
1422758_at	Chst2	2.07	1.33	1.63
1448656_at	Cacnb3	2.07	1.79	1.70
1417928_at	Pdlim4	2.06	1.70	1.72
1450368_a_at	PPP3R1	2.06	1.86	2.41
1420661_a_at	C17ORF39	2.06	2.32	2.54
1424161_at	Ddx27	2.06	2.19	2.19
1440871_at	MAGI1	2.05	1.75	1.68
1454677_at	TIMP2	2.05	1.57	1.36
1422102_a_at	STAT5B	2.05	1.52	1.73
1448185_at	HERPUD1	2.04	1.27	1.36
1418889_a_at	CSNK1D	2.03	1.95	2.57
1416364_at	HSP90AB1	2.02	1.61	1.50
1460661_at	EDG3	2.01	1.90	2.50
1417103_at	DDT	2.01	1.53	1.59
1450632_at	LOC433749	2.00	2.11	2.35
1419746_at	Arhgap23	2.00	1.84	1.95
1426465_at	Dlgap4	2.00	1.67	1.67
1429187_at	Tmed7	2.00	2.15	2.23
1418297_at	Dpysl4	2.00	1.90	2.03
1439051_a_at	MARK4	1.99	1.78	2.01
1424928_at	C11ORF30	1.98	1.97	2.00

1423802_at	Camkv	1.97	1.27	1.13
1456869_at	Zfp787	1.97	1.84	2.07
1453008_at	2300002D11Rik	1.96	1.42	1.49
1416597_at	Hdgfrp2	1.96	1.69	1.65
1421971_a_at	Mrps34	1.95	1.42	1.45
1433921_s_at	Dph3	1.94	2.00	2.33
1429036_at	Otop3	1.94	2.41	3.05
1419753_at	Nfx1	1.90	1.57	1.85
1439375_x_at	ALDOA	1.89	1.79	1.65
1429643_a_at	PDE1C	1.89	1.48	1.39
1434554_at	Trim37	1.88	1.96	2.22
1435117_a_at	RBJ	1.88	1.59	1.29
1436775_a_at	Ankrd17	1.86	1.69	1.56
1427408_a_at	Thrap3	1.86	1.87	2.09
1449263_at	Ufm1	1.86	2.10	2.14
1424914_at	KIAA1737	1.84	1.82	1.59
1450878_at	Sri	1.83	1.53	1.61
1434027_at	Dscr1l2	1.83	1.52	1.67
1434027_at	RCAN3	1.83	1.52	1.67
1426343_at	STT3B	1.82	2.04	2.46
1452730_at	Rps4y2	1.81	1.52	2.03
1421014_a_at	CLYBL	1.79	1.54	1.66
1438016_at	Dkc1	1.79	1.38	1.22
1451364_at	Polr3gl	1.78	1.71	1.68
1460363_at	Tnrc6c	1.78	1.97	1.82
1450472_s_at	SMAD3	1.78	1.38	1.83
1417363_at	Zfp61	1.77	1.91	1.70
1448646_at	Wdr12	1.77	1.60	1.56
1417259_a_at	Capzb	1.77	1.74	1.98
1426306_a_at	Maged2	1.76	1.91	1.85
1460193_at	St13	1.73	2.34	2.73
1433539_at	Commd3	1.71	1.89	1.99
1454987_a_at	H2-Ke6	1.71	1.88	1.73
1415978_at	Tubb3	1.71	1.70	1.72
1417128_at	Plekho1	1.70	1.52	1.50
1424776_a_at	Slc25a28	1.70	1.60	1.49
1418632_at	UBE2H	1.69	1.27	2.07
1422456_at	NSF	1.68	1.46	1.40
1422679_s_at	Ctr9	1.67	2.06	2.07
1435009_at	Slc9a6	1.67	1.64	1.92
1435525_at	Kctd17	1.65	1.40	1.43
1431212_a_at	TRMT6	1.64	2.05	1.92
1427077_a_at	AP2B1	1.63	1.89	2.01
1416284_at	Mrpl28	1.61	1.72	1.66
1415974_at	MAP2K2	1.61	1.71	1.65
1415956_a_at	PCTK1	1.61	1.46	1.80
1427073_at	Lace1	1.61	1.30	1.23
1435698_at	Rictor	1.60	1.48	1.50
1425068_a_at	Tex264	1.60	1.89	1.80
1418432_at	Cab39	1.60	1.60	1.56
1432464_a_at	KIAA1543	1.60	1.43	1.54

1427258_at	Trim24	1.59	1.79	2.00
1427050_at	Txndc16	1.58	1.65	1.66
1422510_at	Ctdspl	1.58	1.28	1.33
1417223_at	Cd2bp2	1.57	1.39	1.34
1417148_at	PDGFRB	1.57	1.47	1.41
1417063_at	C1QB	1.56	2.26	2.57
1453209_at	Brf1	1.55	1.55	1.69
1417504_at	CALB1	1.55	1.26	1.36
1449097_at	TXNRD2	1.55	1.45	1.45
1427149_at	Plekha6	1.55	1.36	1.27
1417870_x_at	Ctsz	1.55	1.79	1.95
1448122_at	Tcp1	1.55	1.62	1.46
1428461_at	PPP2R5E	1.54	1.65	1.68
1456867_x_at	Ergic3	1.53	1.72	1.93
1422489_at	GCS1	1.52	1.73	1.83
1427987_at	Safb2	1.50	1.41	1.14
1416493_at	DDOST	1.50	1.56	1.71
1431137_at	Rusc1	1.47	1.30	1.47
1421148_a_at	Tial1	1.46	1.69	1.98
1452448_at	Aqr	1.46	1.50	1.91
1451048_at	Metap2	1.43	1.62	1.61
1460553_at	1700025K23Rik	1.42	1.75	1.94
1428894_at	Selenoprotein O	1.40	1.54	1.43
1452168_x_at	Gspt1	1.39	2.14	2.25
1432029_a_at	Smap1	1.38	1.60	1.50
1423212_at	Phc1	1.38	1.98	1.86
1451050_at	NT5C3	1.38	1.56	1.63
1429455_at	Gapvd1	1.37	1.78	1.65
1423961_at	Wdr26	1.36	1.98	1.97
1427934_at	Lyrm2	1.32	1.54	1.64
1417258_at	Cct5	1.31	1.54	1.50
1448934_at	NDUFA10	1.31	1.51	1.55
1434894_at	Zc3h13	1.22	1.34	1.26
1423081_a_at	Tomm20	1.17	1.45	1.68
1418528_a_at	Dad1	1.16	1.27	1.28